Atmósfera 39, 107-141 (2025)
https://doi.org/10.20937/ATM.53404

Changes in surface air temperature for Mediterranean climate in Turkey

Buket MESTA[1], Elçin KENTEL[1,2], Hidetaka SASAKI[3,4] and Tosiyuki NAKAEGAWA[3]*

[1] *Department of Earth System Science, Middle East Technical University, 06800 Ankara, Turkey.*
[2] *Department of Civil Engineering, Middle East Technical University, 06800, Ankara, Turkey.*
[3] *Department of Applied Meteorology Research, Meteorological Research Institute, 305-0052, Tsukuba, Japan.*
[4] *Center for Climate Change Adaptation, National Institute for Environmental Studies (NIES), 16-2 Onogawa, 305-8506, Tsukuba, Japan.*
*Corresponding author; email: tnakaega@mri-jma.go.jp

Received: July 29, 2023; Accepted: February 7, 2024

RESUMEN

Las influencias climáticas locales de las masas de agua continentales, la topografía compleja y los mares circundantes hacen que prevalezcan propiedades climáticas templadas, áridas y continentales con variaciones locales en diferentes partes de Turquía. La variabilidad intrarregional de los factores ambientales crea incertidumbres y desafíos en la modelización climática. Este estudio es parte de una investigación sobre los impactos del cambio climático en Turquía que se centra en los impactos sobre la temperatura del aire en la superficie a través de un análisis conjunto de modelos múltiples de modelos climáticos de alta resolución. El conjunto comprende 12 modelos climáticos regionales (RCM, por su sigla en inglés) de EURO-CORDEX y dos modelos del Instituto de Investigación Meteorológica de Japón (MRI). En primer lugar, se validan los datos del modelo histórico con registros de temperatura de 59 estaciones meteorológicas. Además, se analizan los cambios en la climatología de la temperatura en el futuro en horizontes de corto (2020-2030), mediano (2031-2050) y largo plazo (2051-2100) y se comparan con los cambios de precipitación. En el conjunto, dos modelos de resonancia magnética (MRI-AGCM, NHRCM) y dos RCM CORDEX anidados en HadGEM2-ES (RCA4 y CCLM4-8-17) funcionan mejor para replicar la variabilidad espacial de la climatología. El conjunto de 14 componentes proyecta un aumento gradual de la temperatura hasta 4.5 y 6.6 ºC en los escenarios RCP4.5 y RCP8.5, respectivamente. Las proyecciones coinciden en una relación inversa entre los cambios de temperatura y precipitación. Se proyectan impactos más sustanciales en el interior en comparación con las regiones costeras.

ABSTRACT

Local climate influences of inland water bodies, complex topography, and surrounding seas cause temperate, arid, and continental climate properties to prevail with local variations in different parts of Turkey. The intra-regional variability of environmental factors creates uncertainties and challenges in climate modeling. Multi-model ensemble analysis is suggested to be used to characterize the uncertainties and minimize the generalization error in projections. This study is part of a research on climate change impacts in Turkey, focusing on the impacts on surface air temperature through a multi-model ensemble analysis of high-resolution climate models. The ensemble set comprises 12 EURO-CORDEX RCMs and two models from the Japan Meteorological Research Institute (MRI). Firstly, historical model data are validated with temperature records from 59 meteorological stations. Furthermore, changes in temperature climatology in the future in short- (2020-2030), medium- (2031-2050), and long-term (2051-2100) horizons are analyzed and compared with the precipitation changes. In the ensemble, two MRI models (MRI-AGCM, NHRCM) and two CORDEX RCMs nested in the HadGEM2-ES (RCA4 and CCLM4-8-17) perform best to replicate the spatial variability of climatology. The 14-member ensemble projects a gradual increase in the temperature up to 4.5 and

6.6 ºC under RCP4.5 and RCP8.5 scenarios, respectively. The projections agree on an inverse relationship between temperature and precipitation changes. More substantial impacts are projected in inland compared to coastal regions.

Keywords: climate modeling, multi-model ensemble analysis, EURO-CORDEX RCMs, NHRCM, MRI-AGCM, temperature projections.

1. Introduction

The Mediterranean climate, characterized by hot, dry summers and humid, cool winters, is potentially vulnerable to climatic changes (Giorgi and Lionello, 2008) and is expected to be adversely impacted by global climate change (IPCC, 2021). The increase in surface air temperature (hereafter referred to as temperature) is expected to exacerbate the existing anthropogenic-induced pressures on the environment and distinct biodiversity of the region. Giorgi's study (2006) findings corroborate this, characterizing the area as a significant 'hot spot' in terms of its responsiveness to global changes. An increase in the regional temperature is expected to be larger than the increase expected on the global scale. The study indicates a 1.42 ratio of change in regional mean surface air temperature relative to the global average temperature change. A 1.06 ºC increase in global mean temperature observed from 1850 to 2019 created a rise in minimum and maximum temperatures in the Mediterranean basin (Kostopoulou and Jones, 2005; Kuglitsch et al., 2010; Efthymiadis et al., 2011; Bartolini et al., 2012; Tanarhte et al., 2015). Analyses of historical temperature records for temperature changes, heatwaves, and extreme temperature events verified an increasing trend in temperature in Turkey with more evident increase in heatwaves in inland areas in western Turkey, particularly after the 1990s (Tayanç et al., 2009; Cagatan and Unal, 2010; Toros, 2011; Unal et al., 2013; Acar and Gönençgil, 2015; Gönençgil and Acar, 2016; Bayer and Barak, 2017; Erlat et al., 2021; Karadag et al., 2023; Sakalis, 2024).

Regarding the future impacts, Öztürk et al. (2015) studied projections of 16 CMIP3 GCMs for the Mediterranean region under SRES A2, A1B, and B1 scenarios after statistical downscaling, finding an increase in annual temperature (Öztürk et al., 2015). Similarly, analyses of the potential future trends in temperature for different regions of Turkey support the likelihood of a positive anomaly throughout the whole country (Önol and Unal, 2014; Bağçaci et al., 2021). Önol and Unal (2014) gave evidence of a temperature increase within the range of 2-5 ºC by the conclusion of this century through the analysis of projections from the RegCM3 regional climate model driven by the NASA Finite Volume GCM (fvGCM) under the SRES A2 scenario. Bağçaci et al. (2021) made an ensemble analysis of CMIP5 and CMIP6 GCMs and revealed a statistically significant positive anomaly for the near-surface temperature projections for RCP4.5 and 8.5 scenarios.

Assessment of the climate change impacts in the Mediterranean region of Turkey, characterized by intricate topography and climatic attributes, is a challenging task. Previous research verified the existence of variations both between different regions and among different models in the projections produced by CORDEX-RCMs (Aziz et al., 2020). Although studies have given evidence of the potential changes in temperature and precipitation in the Mediterranean basin, only a limited number of studies for Turkey investigate the foreseen size of impacts and potential spatial variabilities (if there are any) within the area. Furthermore, only a few studies comprehensively assess the projection capabilities of different CORDEX RCMs for Turkey.

This study, as part of a research evaluating the climate change impacts in Turkey (Mesta and Kentel, 2021; Mesta, 2022), covers a multimodel ensemble analysis that includes 12 CORDEX models and two climate models developed by the Meteorological Research Institute (MRI) of the Japan Meteorological Agency (JMA), namely the atmospheric general circulation model (AGCM) and the non-hydrostatic regional climate model (NHRCM). The MRI-AGCM has an approximate horizontal grid resolution of 20 km (Mizuta et al., 2006). The NHRCM was created by improving the operational non-hydrostatic model (NHM) from the MRI and the Numerical Prediction Division of the Japan Meteorological Agency

(NPD/JMA). This development is detailed in works by Sasaki et al. (2008, 2011).

To close knowledge gaps in the research region, this paper focuses on the analysis of temperature projections, together with a companion paper (Mesta et al., 2022) on the predictions concerning climate change effects on precipitation. This research is the first study to comprehensively contrast two MRI models with CORDEX RCMs about the eastern Mediterranean basin. The study involves generating NHRCM grid data at a horizontal resolution of 5 km, nested within MRI-AGCM. This nesting strategy is designed to yield projections specifically tailored to the study domain. The NHRCM simulates historical and future (i.e., 1980-2001 and 2080-2100, respectively) climate conditions for timeframes of 20 years. In this study, simulations from 12 CORDEX RCMs, MRI-AGCM, and the NHRCM are initially evaluated for their skill in the simulation of the temperature climatology in the study area. After that, changes in temperature under climate change scenarios are assessed. Finally, a per-basin analysis of the temperature change and its relation to the likely change in precipitation based on the findings by Mesta et al. (2022) is provided.

2. Materials and methods

2.1. Study area

The temperate Mediterranean climate features generally prevail in the study area, encompassing over 200 000 km^2 in southwestern and western Turkey (henceforth referred to as the study area [SA]). The SA includes partially or wholly 10 of the major watersheds, including western, middle, and eastern Mediterranean basins and the surrounding basins (Konya closed, Akarçay, B. Menderes, Burdur, Sakarya, Gediz, and Susurluk; Fig. 1a). In the study area, forests and natural vegetation are the predominant land cover in the coastal basins, while agricultural lands are more common in the inland regions (Fig. 1b). The SA also extends through three regions (Aegean, Mediterranean, and Central Anatolian) of seven separate geographical regions of the country (Fig. 2). Different climatic conditions prevail in each geographical region (Sensoy et al., 2016) due to the effect of the surrounding seas and diverse topography, which has significant control over the regional atmospheric circulation (Lionello et al., 2006).

The Mediterranean region, spanning the majority of western, middle, and eastern Mediterranean basins in Turkey, is separated from the Central Anatolia region by the Taurus mountains stretching parallel to the southern coastline. The Taurus mountains not only form the water divide for the basins in the south but also create a barrier between the regions, creating diversified climatic conditions (Fig. 2). As seen in the Köppen Geiger classification of the SA in Figure 2, the western and southern coastal areas have temperate climate properties typical of the Mediterranean climate. Higher latitude lands of the mountain ranges have cold climate features with dry summers. Behind the barrier of the mountains, continental features dominate the arid steppe climate of Central Anatolia and inland Aegean regions.

2.2 Data

For the validation of the historical projection outputs, the reference data (RD) is obtained from the historical daily mean temperature recordings of the meteorological stations (MSs) located across the SA (Fig. 1). The MSs used for the study are ground-based stations managed by the State Meteorological Services of Turkey. Fifty-nine MSs providing a minimum of 30-year long time series between 1966 and 2005 are selected for the study. The list of the MSs in the SA is given in section S1 in the supplementary material. For assessing the baseline climatology at the SA, annual and seasonal climatological temperature means for each station are computed using the daily mean temperature data.

The assessment of the potential change in temperature due to climate change in the SA involves a multi-model analysis of a 14-member ensemble covering 12 CORDEX RCMs and two MRI models. The list of the climate models is given in Table I. The selection of the GCM/RCM combinations producing 12 high-resolution projections is done to facilitate the evaluation of performance involving a minimum of two distinct RCMs, each utilizing the same GCM as the boundary conditions.

The CORDEX models (0.11º resolution) are acquired from the CORDEX database (ESGF, 2021). The other two model outputs are from high-resolution (0.1875º) AGCM generated by the MRI, and the MRI's NHRCM (5-km resolution). The MRI-AGCM has been used for research regarding future climate

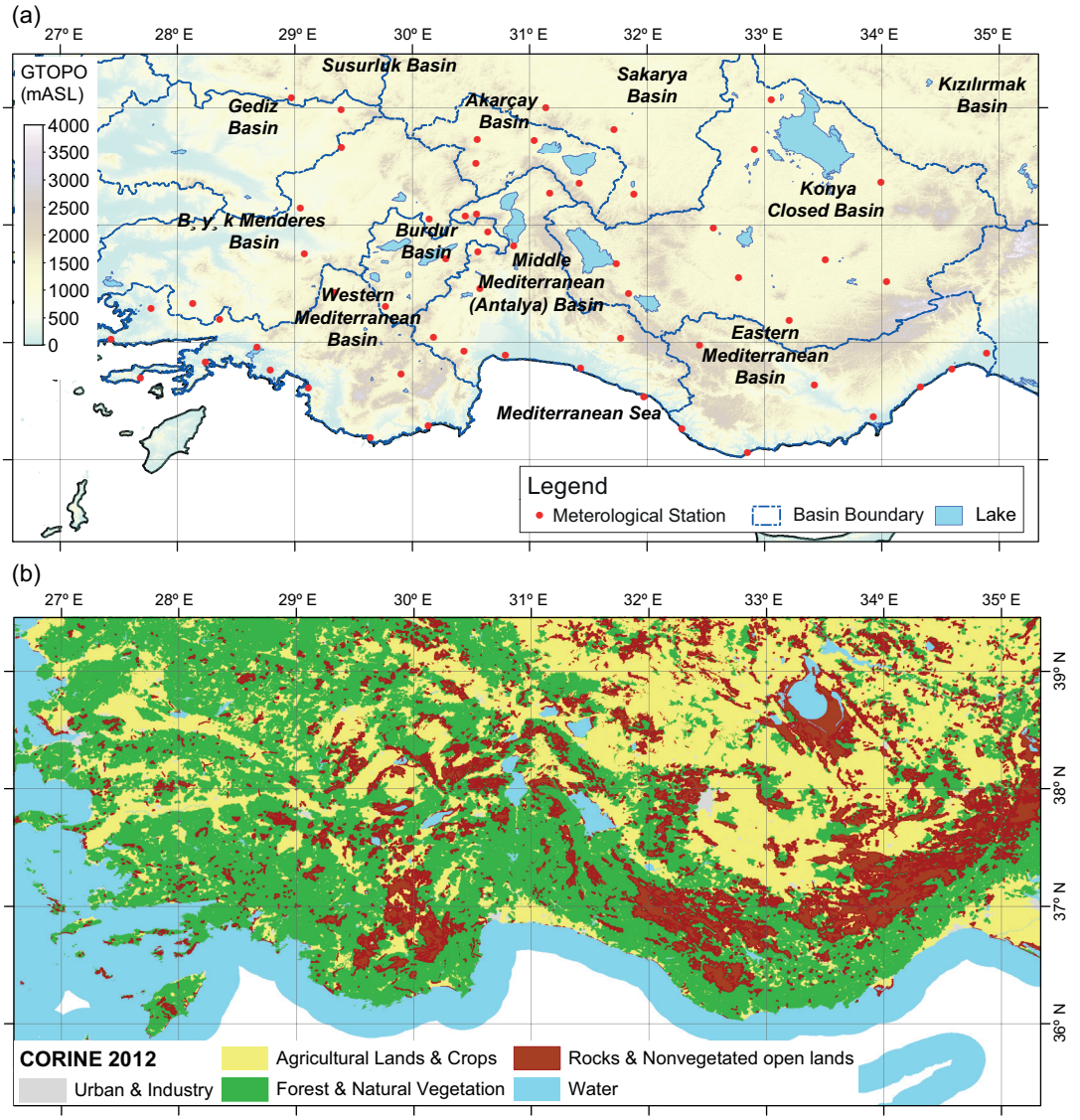

Fig. 1. Study area (SA) topography, land cover properties, and location of 59 meteorological stations in this study. (a) Topography (modified from Mesta et al., 2022), (b) land use/land cover (adapted from EEA-JRC, 2012).

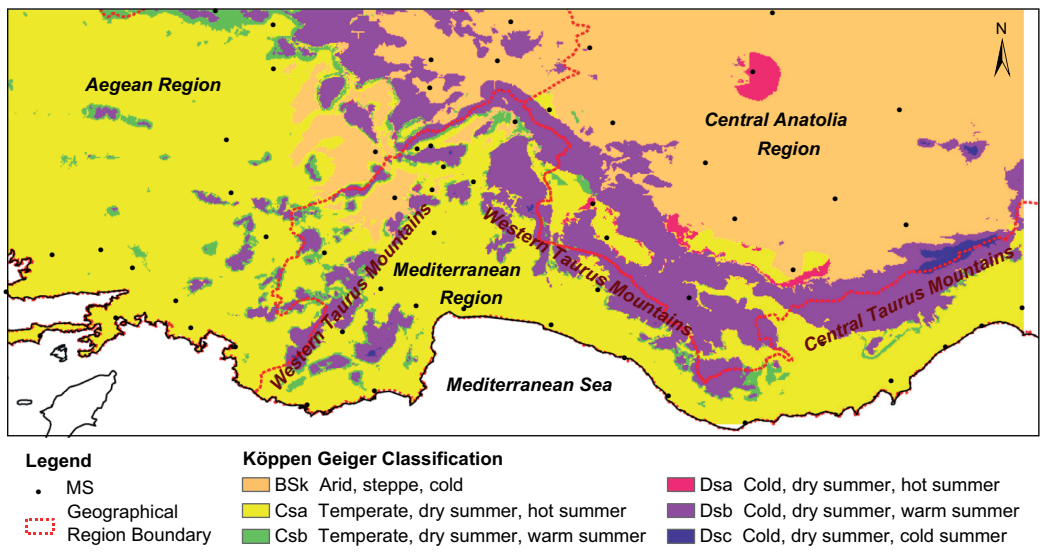

Fig. 2. Map of Köppen Geiger climate zones indicating geographical regions in the study area (adapted from Beck et al., 2018).

Table I. Climate models used in this study (modified from Mesta et al., 2022).

Climate models (RCM/GCM combinations)			Output period		Model resolution	Data source [3,4]	Model ID[5]
Driving GCM and Institution[1]	Name of RCM	Institution (RCM)[2]	Historic	Future scenarios			
MRI_AGCM (MRI)	-	MRI	1979/2003	2075/2100 - RCP8.5	0.1875º	MRI	M1
MRI_AGCM (MRI)	NHRCM (Sasaki et al., 2008, 2011)	MRI	1980/2001	2080/2100 - RCP8.5	5 km	MRI	M2
CNRM_CM5 (CNRM-CERFACS)	ALADIN53 (Colin et al., 2010)	CNRM	1951/2005	2006/2100 - RCP4.5, RCP8.5	0.11º	CORDEX	M3
CNRM_CM5 (CNRM-CERFACS)	CCLM4-8-17 (Rockel et al., 2008)	CLM Community	1950/2005	2006/2100 - RCP4.5, RCP8.5	0.11º	CORDEX	M4
CNRM_CM5 (CNRM-CERFACS)	RCA4 (Kjellström et al., 2016)	SMHI	1970/2005	2006/2100 - RCP4.5, RCP8.5	0.11º	CORDEX	M5
EC_EARTH (ICHEC)	CCLM4-8-17	CLM Community	1949/2005	2006/2100 - RCP4.5, RCP8.5	0.11º	CORDEX	M6
EC_EARTH (ICHEC)	HIRHAM5 (Bøssing et al., 2007)	DMI	1951/2005	2006/2100 - RCP4.5, RCP8.5	0.11º	CORDEX	M7
EC_EARTH (ICHEC)	RACMO22E (van Meijgaard et al., 2012)	KNMI	1950/2005	2006/2100 - RCP4.5, RCP8.5	0.11º	CORDEX	M8
EC_EARTH (ICHEC)	RCA4	SMHI	1970/2005	2006/2100 - RCP4.5, RCP8.5	0.11º	CORDEX	M9
CM5A_MR (IPSL)	RCA4	SMHI	1970/2005	2006/2100 - RCP4.5, RCP8.5	0.11º	CORDEX	M10
CM5A_MR (IPSL)	WRF331F (Skamarock et al., 2008)	IPSL INERIS	1951/2005	2006/2100 - RCP4.5, RCP8.5	0.11º	CORDEX	M11
HadGEM2_ES (MOHC)	CCLM4-8-17	CLM Community	1949/2005	2006/2100 - RCP4.5, RCP8.5	0.11º	CORDEX	M12
HadGEM2_ES (MOHC)	RACMO22E	KNMI	1950/2005	2006/2100 - RCP4.5, RCP8.5	0.11º	CORDEX	M13
HadGEM2_ES (MOHC)	RCA4	SMHI	1970/2005	2006/2100 - RCP4.5, RCP8.5	0.11º	CORDEX	M14

[1] MRI: Japan Meteorological Research Institute, CNRM-CERFACS: National Centre for Meteorological Research of France-Centre for Research and Advanced Training in Scientific Computation; ICHEC: Irish Centre for High-End Computing; IPSL: Institut Pierre-Simon Laplace; MOHC: Met Office Hadley Centre of UK.
[2] MRI: Japan Meteorological Research Institute; CNRM: National Centre for Meteorological Research of France; CLM Community: Climate Limited-Area Modelling Community SMHI: Swedish Meteorological and Hydrological Institute; DMI: Danish Meteorological Institute; KNMI: Royal Netherlands Meteorological Institute, IPSL INERIS: Institut Pierre-Simon Laplace-France National Institute for the Industrial Environment and Risk.
[3] Models with data source from Japan Meteorological Research Institute (MRI).
[4] Models with data source from CORDEX (Coordinated Regional Climate Downscaling Experiment).
[5] Model ID used in this study.

change across different global regions such as Central America and Australia (Nakaegawa et al., 2014, 2017; Kusunoki et al., 2019). The ability of the NHRCM to accurately replicate the precipitation and temperature, extreme storm events, snow depth, storm tracks, and the orographic effect on precipitation has been extensively assessed by multiple studies conducted in Japan (Sasaki and Kurihara, 2008; Sasaki et al., 2008, 2011, 2012, 2013).

2.3 Evaluation of the performance skills of climate models

Climate models are tested for their skills in reproducing baseline climatological conditions. Additionally, their performance is tested for efficiency in replicating the intra-regional variability of climatology regarding temperature in the SA. For the analysis, the annual climatological means of temperature in 59 stations (i.e., the closest modeling grids) calculated from the historical simulations are compared with the observed values. The performance skill is evaluated by using Pearson's correlation coefficient (Corr), root mean square error (RMSE), and bias (Bias) indicators calculated using the annual mean temperature data series in degrees Celsius.

In addition, for each model, a performance index is calculated to determine the best climate models for the SA in terms of efficiency in temperature simulation. The models are ranked three times for each indicator to compute an aggregated performance index (API). This involves arranging all models from best- to worst-performing for each indicator and then averaging the three ranks assigned to each model. The lowest API value is accepted to indicate the highest modeling skill for the SA. Eq. (1) below is used for the calculation of API values for model n.

$$API_n = \frac{\sum_{i=1}^{3} R_{n,i}}{3} \quad (1)$$

where $R_{n,i}$ is the ranking of model n with respect to the statistical performance indicators i (here i is Corr, RMSE, or Bias).

The climate models in the multimodel and mean ensembles are used for the determination of the potential future changes in temperature climatology. The statistical significance of potential change indicated by individual models is tested by the use of Welch's two-sample t-test.

The baseline temperature climatology for the reference period and projections of temperature changes from individual models and the mean ensemble are illustrated using maps. These maps are created from data provided by 59 MSs, utilizing the inverse distance weighted (IDW) interpolation method to generate surficial data. IDW is a widely used technique for creating spatial distribution maps, where the spatial values are derived from the weighted average of nearby observations, with weights determined by the Euclidean distance between points (Kurtzman and Kadmon, 1999; Setianto and Triandini, 2013; Yang et al., 2020). This study uses an inverse distance power of 2 for the IDW method.

3. Results and discussion

3.1. Temperature climatology analysis

The RD from 59 MSs is used to assess the annual and seasonal climatological means of temperature ($\overline{T_{annual}}$ and $\overline{T_{seasonal}}$, respectively) in the SA. $\overline{T_{annual}}$ is the long-term mean of the annual means of daily average temperatures for each MS. Similarly, $\overline{T_{seasonal}}$ is the long-term mean value of the seasonal temperature means. In order to obtain the climatology maps for the SA, $\overline{T_{annual}}$ values of MSs are processed through the IDW interpolation method to obtain a spatial distribution across the SA. Figure 3 displays the relevant climatology maps. The $\overline{T_{annual}}$ values range between 10 and 20 ºC (Fig. 3a) in the SA. In fact, for coastal MSs, $\overline{T_{annual}}$ values are greater than or equal to 18 ºC, whereas, for the remaining two-thirds of the MSs, located inland, they are between 10 and 17 ºC (Fig. 4). The highest and lowest $\overline{T_{annual}}$ values are observed at the coastal Kas MS (MS 17380; see Table SI in the supplementary material) in the Middle Mediterranean basin, and the inland Hadim MS (MS 17928) in the Eastern Mediterranean basin, respectively (Fig. 4). The coastal stations also have the highest $\overline{T_{seasonal}}$ values for all seasons in the region. The areal average of temperature means (the average of climatological temperature means for the 59 MSs) for the winter season (December, January, February) $\overline{T_{DJF}}$ is 5 ºC. $\overline{T_{DJF}}$ ranges between –1 ºC at Kulu MS (17754) and 13 ºC (at Kas MS, 17380) (Fig. 3b), whereas the climatological summer (June, July, August) temperature mean $\overline{T_{JJA}}$ at the MSs in the SA ranges between 19 ºC at Hadim MS (17928) and 28 ºC at Mut MS (17956) (Fig. 3d).

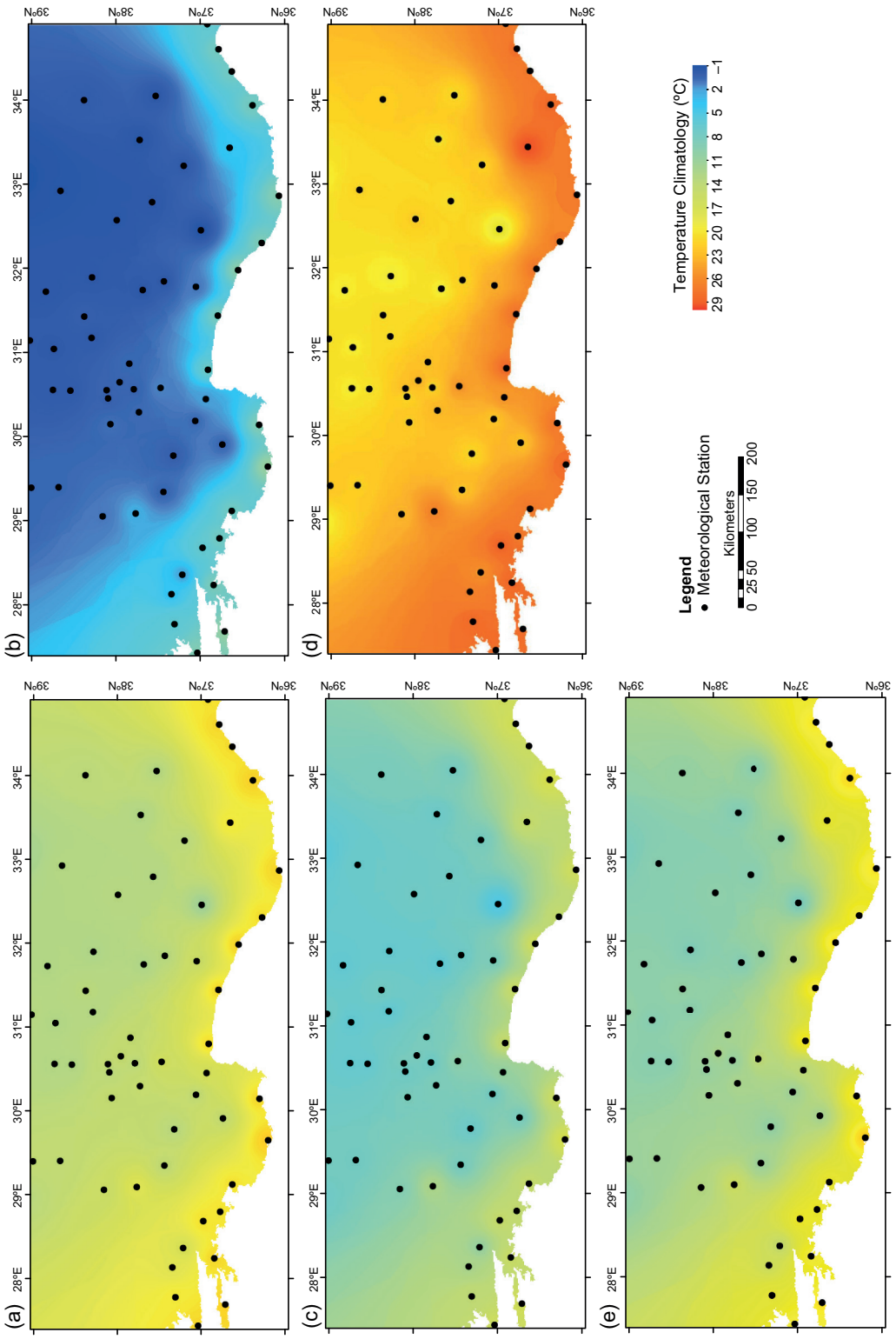

Fig. 3. Intra-regional variability of temperature climatology: (a) annual; (b) winter (December, January, February); (c) spring (March, April, May); (d) summer (June, July, August); (e) fall (September, October, November).

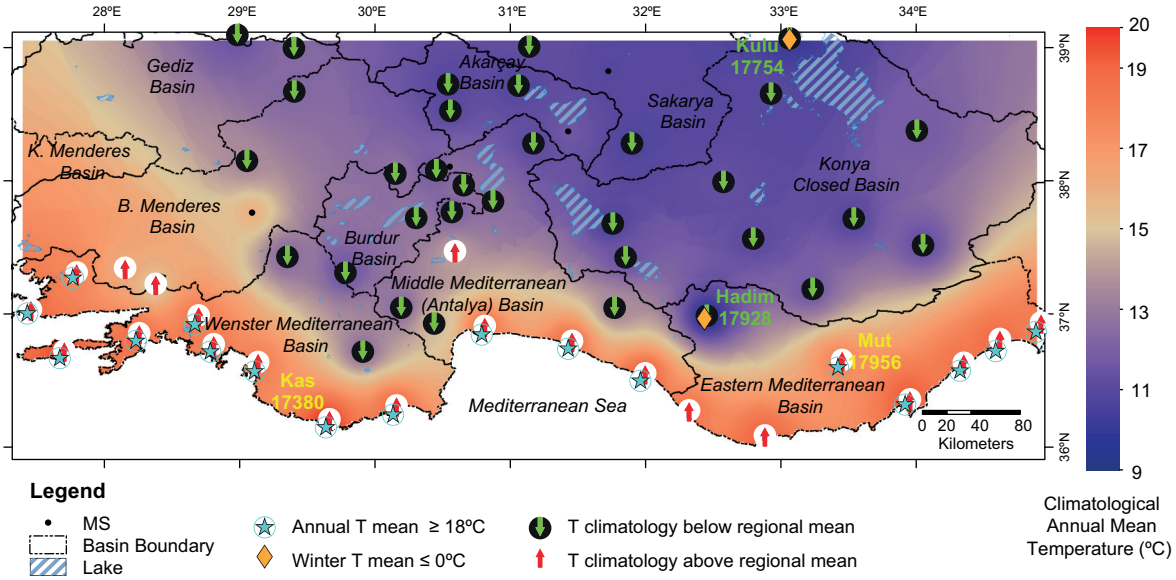

Fig. 4. $\overline{T_{annual}}$ and $\overline{T_{seasonal}}$ variability in the study area.

3.2. Analysis of the modeling performance

The performance of climate models in simulating accurate results is tested through a benchmark of RD from 59 MSs with the historical simulations at the closest modeling grids. Individual performance indicators (Corr, RMSE, and Bias) and APIs are calculate by the comparison of the simulated and observed $\overline{T_{annual}}$ at MSs in order to identify the simulation skills in representing spatial variability of temperature in the SA. The results are given in Table II. Accordingly, all models in the ensemble attain high Corr values ranging between 0.86 and 0.94 to replicate

Table II. Calculated values of the performance indicators.

Model ID	Climate model	Corr	RMSE (ºC)	Bias* (ºC)	API
M1	MRI_AGCM	0.89	**1.58**	**0.05**	5.00
M2	NHRCM	0.90	1.61	0.73	5.33
M3	CNRM_CM5 ALADIN53	0.86	4.69	4.15	14.00
M4	CNRM_CM5 CCLM4-8-17	0.92	2.83	2.39	8.67
M5	CNRM_CM5 RCA4	0.93	2.90	2.59	9.00
M6	EC_EARTH CCLM4-8-17	0.93	2.68	2.30	7.67
M7	EC_EARTH HIRHAM5	0.92	2.00	1.29	5.67
M8	EC_EARTH RACMO22E	**0.94**	4.08	3.80	9.33
M9	EC_EARTH RCA4	**0.94**	3.45	3.23	9.00
M10	CM5A_MR RCA4	0.93	2.59	2.28	6.00
M11	CM5A_MR WRF331F	0.90	2.62	2.16	8.00
M12	HadGEM2_ES CCLM4-8-17	0.91	1.82	1.06	5.33
M13	HadGEM2-ES_RACMO22E	**0.94**	3.04	2.58	7.33
M14	HadGEM2-ES_RCA4	**0.94**	2.20	1.79	**4.67**

*Mean difference between observed and simulated.
Corr: Pearson's correlation coefficient; RMSE: root mean square error.
Best values are written in bold.

the spatial variability of $\overline{T_{annual}}$, as can be seen in the Taylor diagram in Figure 5. In general, relatively similar simulation efficiencies are observed for the 14 models except for M3, which is verified to perform weaker than other models.

Taking the API values into consideration, five models show the highest simulation skills in modeling the spatial variability of $\overline{T_{annual}}$. These are two MRI models (M1 and M2), two RCMs (M14 [RCA4] and M12 [CCLM4-8-17]) using HadGEM2-ES as driving GCM, and M7 (HIRHAM5) nested in EC-EARTH. On the other hand, M3 (ALADIN53 nested in CNRM-CM5) has the weakest performance value among the 14 climate models. Indeed, the weak performance of ALADIN53 can be attributed to problematic sea surface temperature (SST) mapping from driving GCMs as indicated in the EURO-CORDEX's technical errata webpage (EURO-CORDEX, 2021).

Among the best-performing five models, in addition to the MRI models, the driving GCMs for the CORDEX RCMs are HadGEM2-ES and EC-EARTH. On the other hand, in the SA, the worst-performing five models are nested in EC-EARTH and CNRM-CM5. The projection skill of EC-EARTH for temperature varies depending on the RCM. Thus, the diminished proficiency of RCMs using CNRM-CM5 could potentially be linked to issues with boundary-forcing conditions during historical runs. The potential influence on the model outcomes has been reported by EURO-CORDEX (2021). Furthermore, not including the forcing agent of land-use change that forms one of the primary climate forcings (Mahmood et al., 2010) in the model setup (Collins et al., 2013; Boé et al., 2020) is another potential reason for the relatively lower performance of CNRM-CM5 for the SA in temperature simulations as well as in the simulation of precipitation climatology, as verified by an earlier study of Mesta et al. (2022).

The multi-model ensemble analysis by Mesta et al. (2022), using the same climate models investigating the model performances and potential changes regarding precipitation for the same study area, verified that NHRCM nested in MRI-AGCM has a similar high skill in replicating the climatological intra-regional variability of precipitation. Unlike temperature simulations, the simulation skill for precipitation climatology depends on the RCMs nested in HadGEM2-ES, whereas RCMs (i.e., HIRHAM5, CCLM4-8-17, RACMO22E, and RCA4) using EC-EARTH as the driving model perform well for precipitation (Mesta et al., 2022).

Analysis of the models' performances for the replication of the intra-regional variability of $\overline{T_{seasonal}}$

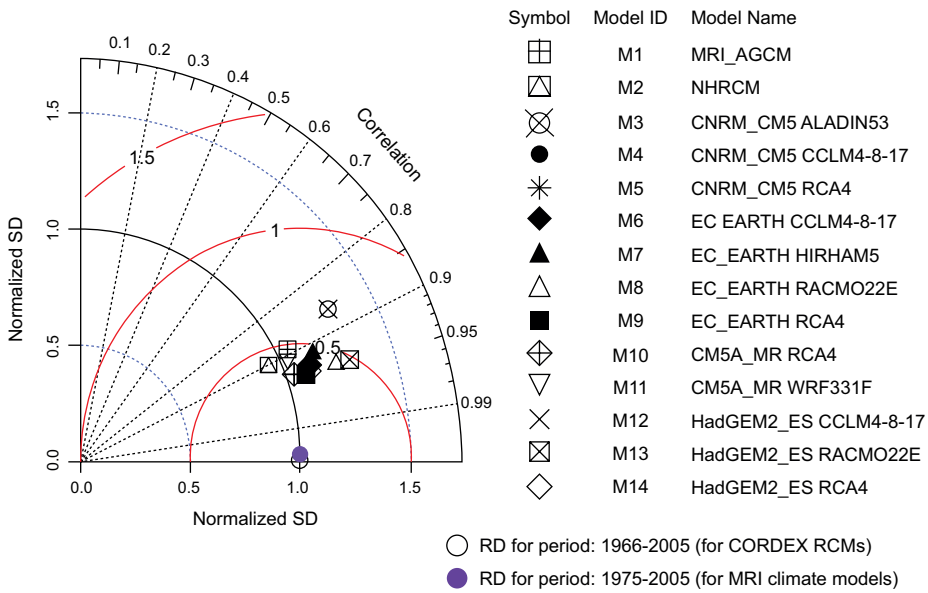

Fig. 5. Taylor diagram of climate models.

shows the highest Corr values for winter and the lowest for summer for all climate models in the ensemble. Twelve CORDEX RCMs are seen to underestimate the temperature climatology in the SA for all seasons (see section S.2 in the supplementary material).

3.3. Future projections on temperature

Temperature projections obtained from 12 CORDEX RCMs for short- (2020-2030), medium- (2031-2050), and long-term (2051-2100) horizons are analyzed by comparing the future simulation outcomes with the $\overline{T_{annual}}$ of the reference period. The outcomes of two high-resolution MRI models are also compared for the 20-year future timeframe between 2080 and 2100 under the RCP8.5 scenario.

The following equations are used to calculate the projected change in temperature:

$$\textit{Change in annual temperature climatology } (\Delta T_{annual}) = T - \overline{T_{annual}} \quad (2)$$

$$\textit{Change in seasonal temperature climatology } (\Delta T_{seasonal}) = T - \overline{T_{seasonal}} \quad (3)$$

where ΔT_{annual} and $\Delta T_{seasonal}$ are the differences in $\overline{T_{annual}}$ and $\overline{T_{seasonal}}$ between the reference period and the future projection period, T. Maps in Figures 6 to 11 show the ΔT_{annual} projections of CORDEX models' ensemble mean (EM) for each projection period in the SA to depict the areal variability of projected changes. The projections by individual CORDEX models in the ensemble are provided in section S2 (Figs. S1-6). Additionally, for the long-term future scenario under RCP8.5 (Fig. 11), two ensemble means are generated, the first using only 12 CORDEX RCMs and the second using two MRI models (M1, and M2) and 12 CORDEX RCMs. The areal data used to produce these maps are generated with the IDW interpolation method with projections for the modeling grids. A summary of the projections' range by the ensemble is given in Table III.

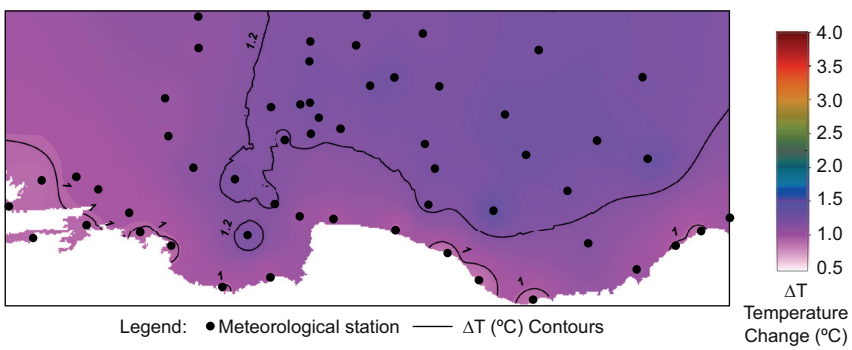

Fig. 6. Map of ensemble means (EMs) of short-term projections (RCP4.5) for temperature change (ΔT_{annual} [ºC]) from 12 CORDEX RCMs.

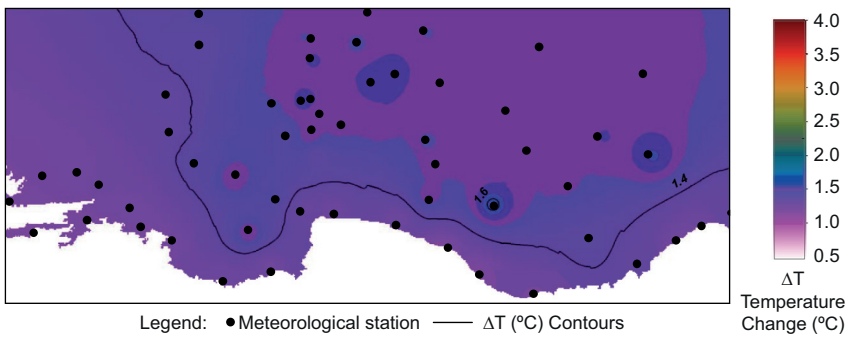

Fig. 7. Map of ensemble means (EMs) of short-term projections (RCP8.5) for temperature change (ΔT_{annual} [ºC]) from 12 CORDEX RCMs.

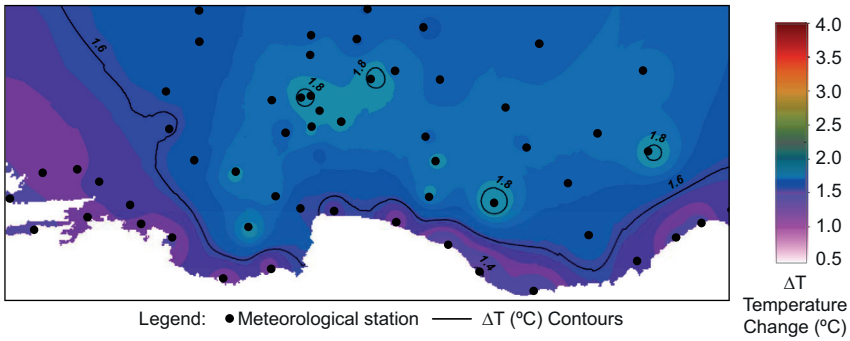

Fig. 8. Map of ensemble means (EMs) of medium-term projections (RCP4.5) for temperature change (ΔT_{annual} [ºC]) from 12 CORDEX RCMs.

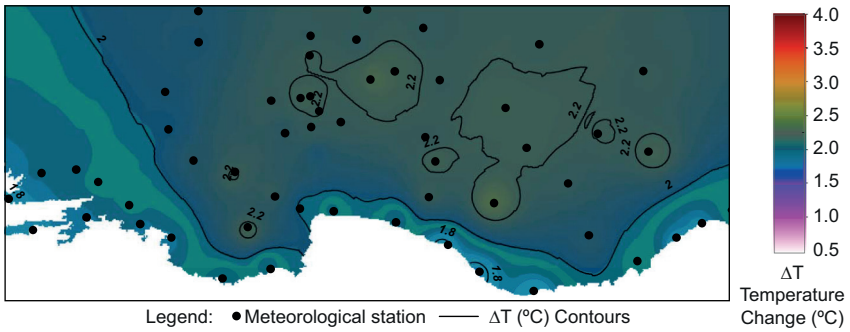

Fig. 9. Map of ensemble means of medium-term projections (RCP8.5) for temperature change (ΔT_{annual} [ºC]) from 12 CORDEX RCMs.

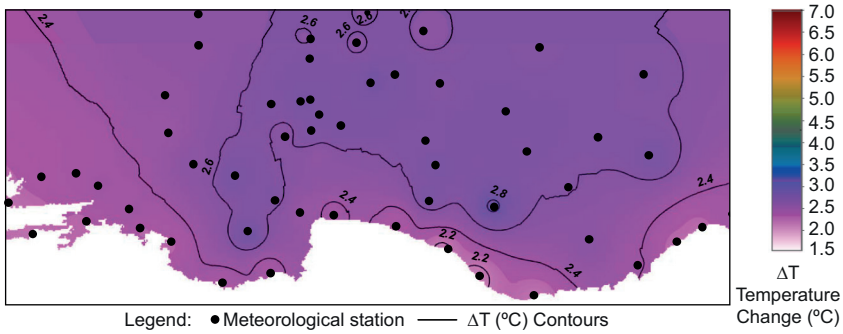

Fig. 10. Map of ensemble means of long-term projections (RCP4.5) for temperature change (ΔT_{annual} [ºC]) from 12 CORDEX RCMs.

To test the significance of ΔT_{annual} at a 95% confidence level, the annual temperature projections are tested against the reference period using Welch's two-sample t-test, which is used for the projections of individual models and not for the ensemble mean. The t-test indicates that all models agree on a statistically significant increase of $\overline{T_{annual}}$ in the entire SA with a 95% confidence level. On the other hand, regarding the precipitation climatology in the SA, the statistical significance of change in the long-term future scenario under RCP 4.5 is identified to be limited to approximately 30% or less of the MSs, whereas for RCP8.5, the change is statistically significant for over 60% of the MSs in the SA (Mesta et al., 2022).

As seen in Figures 6 and 7, for the short-term, EM projects a relatively higher temperature increase

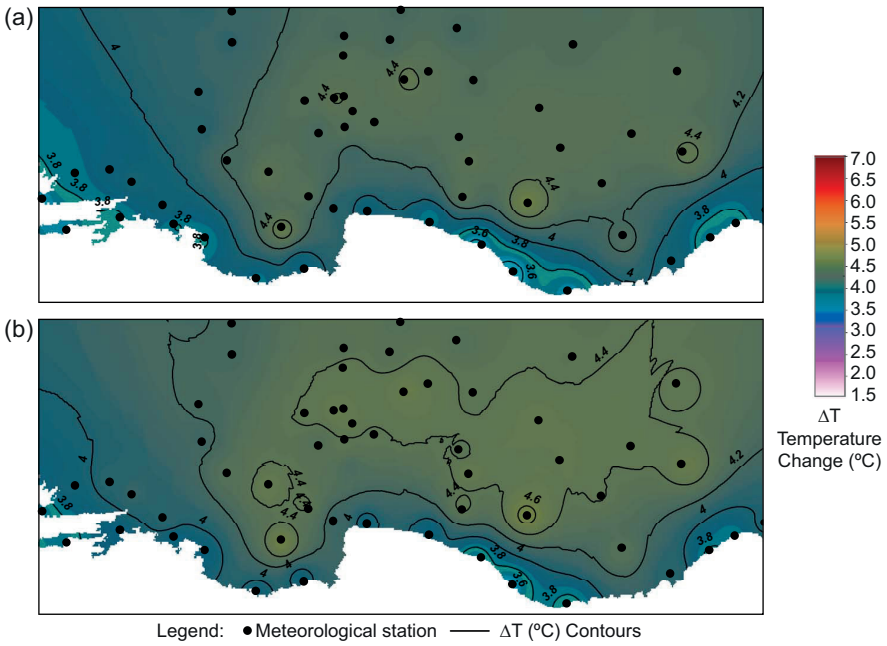

Fig. 11. Map of ensemble means showing long-term projections (RCP8.5) for temperature change (ΔT_{annual} [ºC]). (a) Ensemble means of projections from 12 CORDEX RCMs; (b) ensemble means of projections from 14 climate models.

for inland areas than coastal ones. A similar projection by the EM on a higher temperature increase for inland MSs than for coastal areas is apparent for other future periods. The higher increase in temperature in inland areas is considered to have originated from the reduction of evaporative cooling due to the diminished soil moisture content in those areas. The amplified increase in temperatures in dryer climate in inland parts of the SA is interpreted to be connected with several physical mechanisms (including the increase in dryness and added positive feedback of subsequent decrease in cloud formation) that exacerbate the solar radiation effect (Zampieri et al., 2009; Seneviratne et al., 2010, 2013). Regarding the impact on temperature combined with local climate processes, Zittis et al. (2014) verified a strong inverse correlation between soil moisture and temperature in the Balkans and Turkey in the areas situated north and south of the Caucasus Mountains. Furthermore, Zittis and Hadjinicolaou (2016) demonstrated that increasing temperatures are related to reduced cloud cover, resulting in higher solar short-wave radiation reaching the surface.

The potential evaporative cooling impact at the coastal stations is in line with the topographical features, which is seen to be represented particularly in the projections by M8 through M14 (see Fig. S7 in section S3 of the supplementary material). The effect of the Mediterranean Sea is prevalent along the southern shoreline bordered by the impediment of the Taurus Mountains. In contrast, on the western coast of the Aegean region, the effect of the sea is seen to reach farther inland due to the stretch of mountains perpendicular to the shoreline, which maintains a farther outreach for westerly flow (Önol and Unal, 2014). In general, this is more evident in the projections by RCA4 (M9, M10, and M14 in Fig. S7).

Regarding the future projections depicted in Figures S7 through S12, for both RCP4.5 and RCP8.5 scenarios, CM5A-MR and HADGEM2-ES as the driving GCMs of RCMs in the ensemble project a more significant temperature increase compared to CNRM-CM5 and EC-EARTH. The projections of models nested in CNRM-CM5 on relatively lower severity of temperature increase might be linked to the model setup, which does not include the forcing of land-use change.

Table III. Summary of the projections on temperature change, ΔT_{annual} (ºC).

	2020-2030			2031-2050			2051-2100		
	RCP4.5	RCP8.5		RCP4.5	RCP8.5		RCP4.5	RCP8.5	
Max MR* (12 RCMs)	0.6-2.6	**(0.7-2.0)**	0.9-2.7	**(1.0-2.2)**	0.9-3.3	**(1.1-2.7)**	1.2-4.1	**(1.3-3.3)**	1.7-4.5	**(1.9-3.7)**	2.8-6.6	**(3.2-5.5)**
Mean MR** (EM)	0.9-1.4	**(1.2)**	1.2-1.6	**(1.4)**	1.4-1.8	**(1.6)**	1.8-2.3	**(2.1)**	2.1-2.8	**(2.5)**	3.5-4.6	**(4.1)**
Best RCM M14	1.3-2.1	**(1.6)**	1.6-2.1	**(1.7)**	1.9-2.7	**(2.3)**	2.4-3.2	**(2.7)**	2.7-3.6	**(3.2)**	4.2-5.4	**(4.8)**

*Maximum range for change in temperature in 59 MSs projected by 12 RCMs; **Range of the projections on temperature change across the SA by the EM of the 12-member ensemble.
RCM: regional climate model; MR: model range; EM: ensemble mean.
Values in brackets written in bold indicate SA means.

A summary of the ΔT_{annual} projections is given in Table III, where the SA means calculated for 12 models, EM, and M14, are shown in brackets. Accordingly, the best-performing CORDEX RCM (M14) projects a higher ΔT_{annual} in the SA than the EM for all future periods under both scenarios.

The long-term projections on ΔT_{annual} by two MRI models are shown in Figure 12. Accordingly, M1 projects a slightly higher temperature increase for most MSs than M2. The areal average temperature increase is projected as 4.9 ºC by M1 and 4.7 ºC by M2. Hence, MRI models project a slightly higher SA average for temperature increase than the mean of the 12 CORDEX models. Like CORDEX RCMs, both MRI models project statistically significant changes in temperature in the entire SA. The analysis of MRI's NHRCM projection regarding the change in precipitation climatology in the SA indicates that for over 40% of the MSs, the change is statistically significant (Mesta et al., 2022).

Although all models agree on a gradual increase in $\overline{T_{annual}}$ across the entire SA under both scenarios, inter-model variability is still noticeable, particularly regarding the intensity of the impact. Among the models in the ensemble, RACMO22E displays the highest spatial variability in the impact as well as the most distinct difference between the two scenarios, whereas HIRHAM5 and CCLM-4-8-17 project relatively lower variability under both scenarios. Under the RCP4.5 scenario, most of the models agree on a decline in the rate of increase in temperature (increase per decade) for the latter half of the century (i.e., long-term future scenario). Under RCP8.5, all models except the RCMs nested in HadGEM2-ES, project a relatively higher per decade rate of increase period in temperature for more than half or the entire SA for the long-term scenario (see Figs. S7 through S12 in section S3 of the supplementary material).

The diversity in projections among different models is attributed to the divergence in the model setups of RCMs in the ensemble due to different approaches to the forcing connected with changes in GHGs and aerosols in time (Jerez et al., 2018; Gutiérrez et al., 2020; Sørland et al., 2020). The box plots in Figure 13 show the range of projections calculated for the member models in the ensemble for both RCP4.5 and RCP8.5 scenarios for the short-, medium- and long-term future periods.

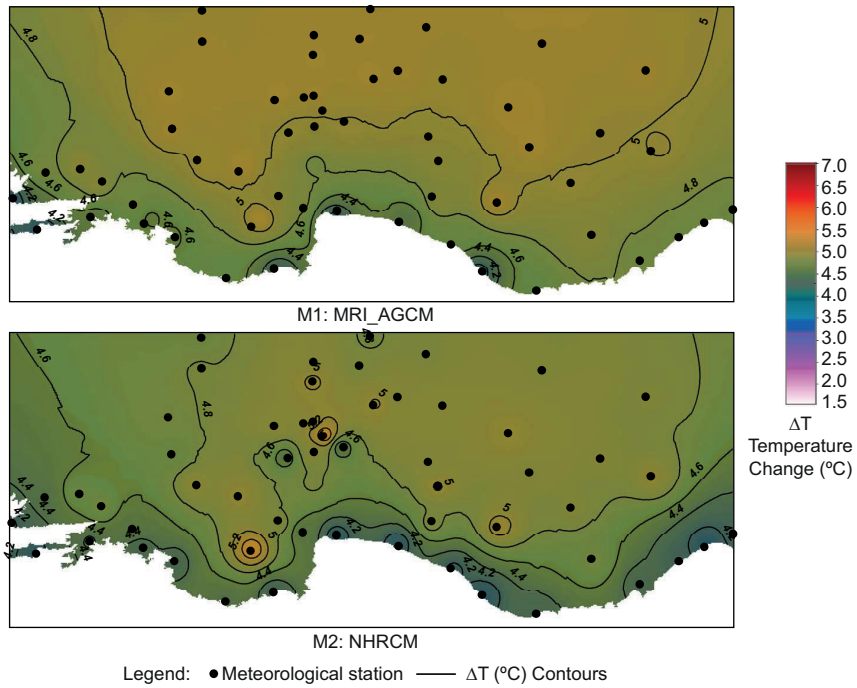

Fig. 12. Long-term projections (RCP8.5) for temperature change (ΔT_{annual} [ºC]) from MRI climate models for M1 and M2. All changes are verified to be statistically significant at the 95% confidence level.

Table IV summarizes the $\Delta T_{seasonal}$ projections for RCP4.5 and RCP8.5 scenarios in the SA. The box plots are given in section S3 of the supplementary material. For the long-term scenario (2080-2099), MRI climate models project a 3.8 ºC increase for winter, similar to the CORDEX RCMs. For the summer, the increase projected by MRI models is 6 ºC, which is at the highest end of the range of projections by 12 CORDEX RCMs.

Figure 14 shows the average ΔT_{annual} per basin and for the entire study area as projected by the mean of the 14-member ensemble for the short-, medium- and long-term future. Accordingly, a gradual increase in temperature is projected for scenarios RCP4.5 and RCP8.5 by the end of the current century. Four of the inland basins (Konya, Akarcay, Burdur, and Sakarya) located behind the topographical boundary formed by the Taurus Mountains are projected to have a slightly higher temperature increase than the general average of the study area for both scenarios and throughout the entire century from short- to long-term.

The amplified temperature increase in inland regions with continental climate characteristics is expected to result from the intensification of drought conditions. The soil moisture controls the sensible to latent heat flux ratio, particularly for dry climates and transitional climates between dry and wet (Seneviratne et al., 2010). Increased dryness decreases the latent heat flux and the cooling effect of evaporation but increases the sensible heat flux that, in turn, escalates the surface temperature. Haarsma et al. (2009) verified that elevated surface air temperature in the Mediterranean region causes a decline in latent heat flux, although the surface solar radiation remains relatively stable. The increase is related to low soil moisture in the semi-arid conditions of the Mediterranean region (Haarsma et al., 2009). The control of soil moisture and climate change-induced dryness is verified to have a strong effect on mean temperature and even on mean precipitation; however, precipitation findings are more uncertain (Seneviratne et al., 2013). For areas such as Central Anatolia, which has a semi-arid steppe climate, evapotranspiration is very limited but closely correlated with soil moisture. A decrease in soil moisture due to increasing temperature forms positive feedback for the elevated

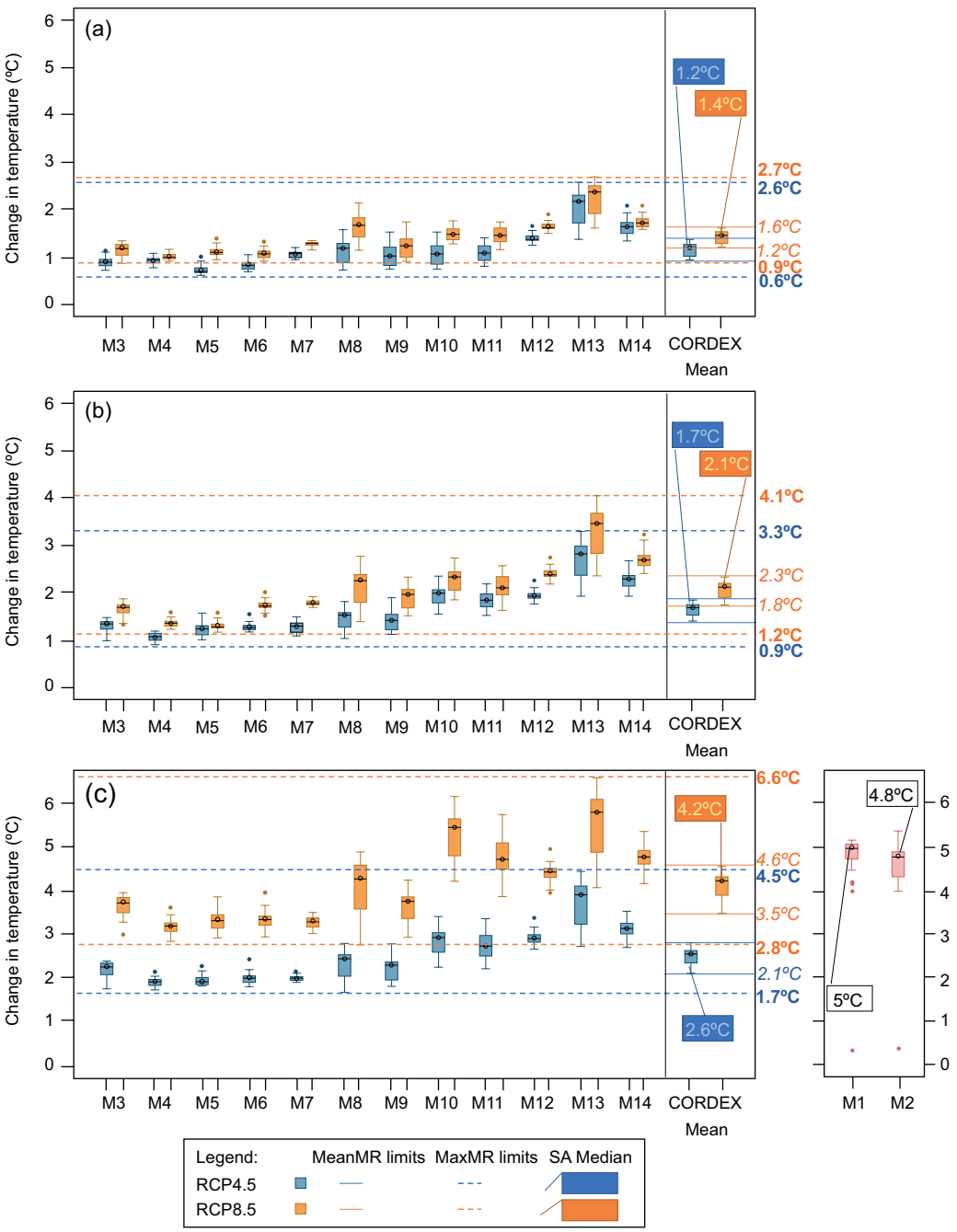

Fig. 13. Boxplots of temperature change (ΔT_{annual} [ºC]) projections (RCP4.5 and RCP8.5): (a) short-term period; (b) medium-term period; (c) long-term period. MRI's AGCM and NHRCM boxplots apply only to the RCP8.5 scenario. Because of the dissimilarity in the projection timeframes, the results from MRI-AGCM and NHRCM are presented distinctly from the CORDEX RCMs (the upper whisker boundary extends to the largest data point within 1.5 times the interquartile range [IQR] above the third quartile, while the lower whisker boundary extends to the smallest data point within 1.5 times the IQR below the first quartile).

Table IV. Seasonal temperature change, $\Delta T_{seasonal}$ (ºC) values for CORDEX RCMs.

	2020-2030				2031-2050				2051-2100			
	RCP4.5		RCP8.5		RCP4.5		RCP8.5		RCP4.5		RCP8.5	
Winter	0.5-2.3	**(1.3)**	0.9-2.4	**(1.4)**	0.9-2.9	**(1.7)**	1.1-3.7	**(2.0)**	1.8-3.8	**(2.4)**	2.8-5.4	**(3.7)**
Spring	0.5-2.3	**(1.1)**	0.6-2.5	**(1.4)**	0.6-3.0	**(1.6)**	1.0-3.4	**(2.0)**	1.6-4.1	**(2.5)**	2.7-5.9	**(4.1)**
Summer	0.9-2.2	**(1.4)**	1.2-2.0	**(1.6)**	1.3-2.8	**(2.0)**	1.4-3.3	**(2.3)**	2.2-3.8	**(2.8)**	3.9-6.0	**(4.7)**
Fall	0.3-1.6	**(1.0)**	1.2-2.3	**(1.6)**	1.0-2.5	**(1.6)**	1.7-3.2	**(2.2)**	2.0-3.5	**(2.6)**	3.3-5.3	**(4.1)**

Values in brackets written in bold indicate the ensemble mean of 12 CORDEX regional climate models (RCMs).

temperatures (Haarsma et al., 2009; Seneviratne et al., 2010, 2013; Byrne and O'Gorman, 2018; Selten et al., 2020). Due to limited evapotranspiration, the offset of the drop by enhanced precipitation in soil moisture is not possible. Furthermore, for transitional soil moisture regime or climate (between dry and wet) conditions, soil moisture plays an even more critical role in increasing climate variability (Seneviratne et al., 2013). Hence, projections for a heightened temperature increase in inland areas and the intra-regional variability pattern of the impact on temperature in the study area, which is particularly displayed by RACMO22E, RCA4, WRF331F, ALADIN53, MRI-AGCM, and NHRCM, follow the influence of major local climate drivers.

3.4. Comparison of changes in temperature and precipitation climatologies

The potential short-, medium- and long-term changes in precipitation in the SA have been previously studied by Mesta et al. (2022). The correlation between ΔT_{annual} and percent change in precipitation according to the average of 12 CORDEX RCMs, and NHRCM as the areal average of each basin under RCP 4.5 and 8.5 scenarios is examined through the graph in Figure 15. The relation between change in precipitation and temperature in the long term, according to the projection of MRI-AGCM, is shown in Figure 16.

As seen in Figure 15, all RCMs project an inverse linear relationship between temperature and precipitation changes at basins and, on average, the entire SA. For the long-term scenario, projections indicate a consistent trend across all sub-basins: a decrease in precipitation alongside an increase in temperature. These two simultaneous changes in climate may cause amplified stress on the SA water resources. The results of short-, medium- and long-term projections in precipitation and temperature demonstrate the need for tiered adaptation measures to climate change. The analysis also indicates that the sensitivity of climate models to two scenarios will be higher in the long term. The magnitude of the impact becomes distinctly higher for the long-term projection, and the variability increases between the two scenarios compared to the short-term scenario, in which projections concentrate around the regional mean for all basins.

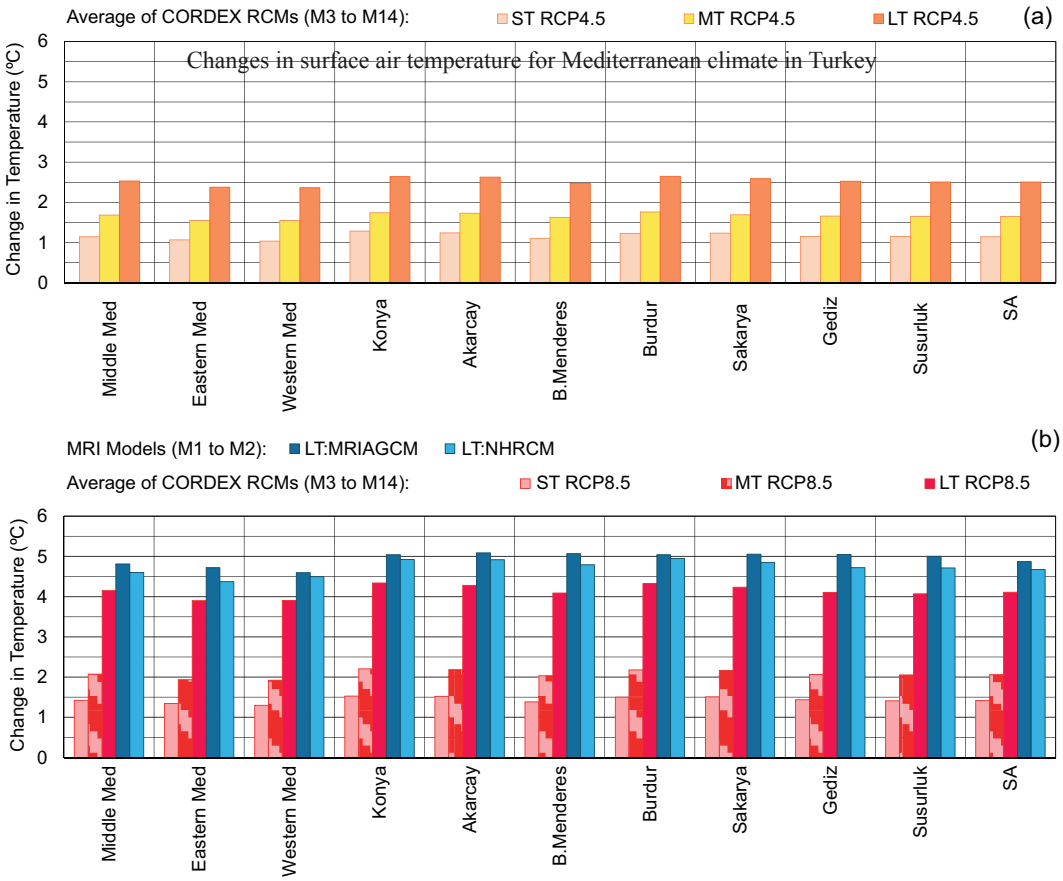

Fig. 14. Areal average of ΔT_{annual} projections for basins in the study area regarding the short-, medium-, and long-term future scenarios relative to the historic period. (a) RCP4.5; (b) RCP8.5.

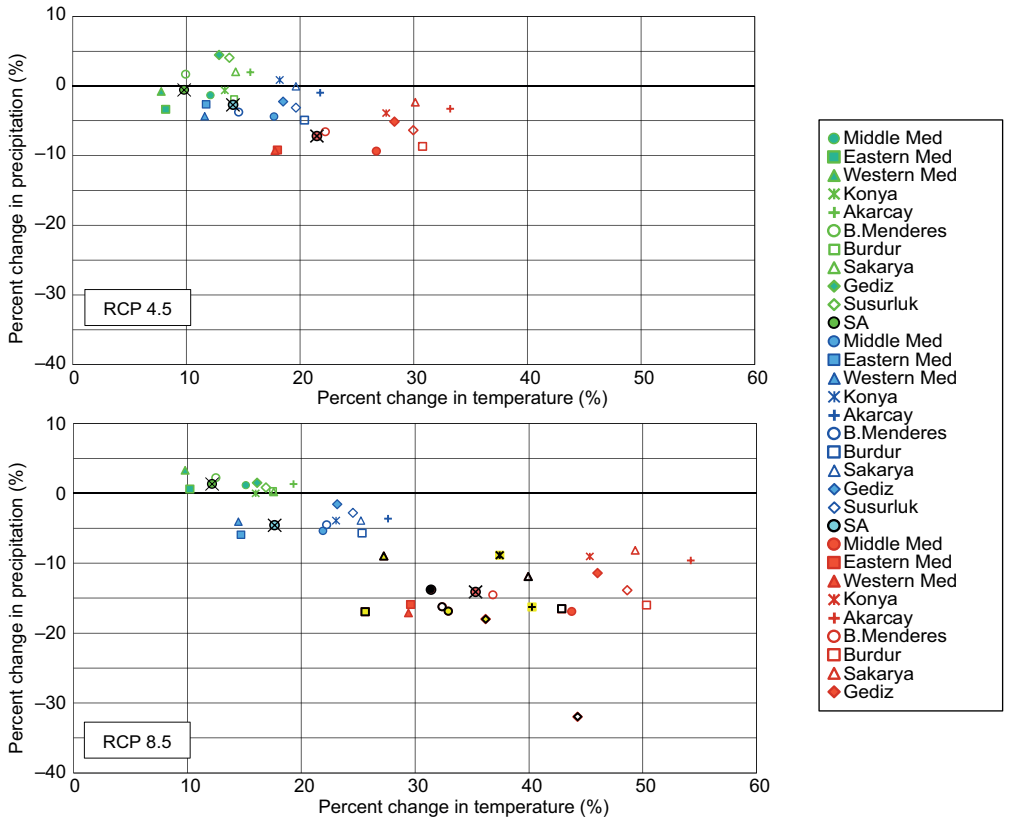

Fig. 15. Areal average changes at basins in the study area projected for the short-, medium-, and long-term scenarios based on the average projection by 12 CORDEX models, and projection by NHRCM.

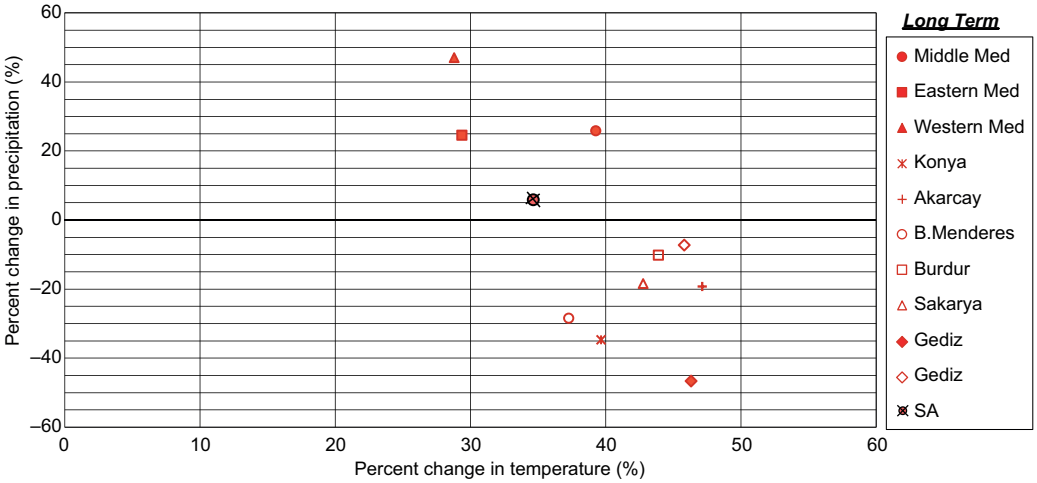

Fig. 16. Areal average changes at basins in the study area for the long-term scenario projected by MRI-AGCM (RCP8.5 only).

The projections of MRI-AGCM indicate an increase both in precipitation and temperature in the long term for the Mediterranean region of Turkey, including the west, middle, and east Mediterranean basins stretching along the Mediterranean coastline (see Fig. 16). On the other hand, for inland basins, around 40-50% temperature increase concurrent to various levels of decrease in precipitation in the range of 5-50% is projected. The projections by MRI-AGCM are explained by a potential increase in precipitation due to elevated evapotranspiration in coastal areas, where the relative moisture is generally higher. However, precipitation in areas where semi-arid continental climate features prevail is expected to drop even more due to soil moisture depletion.

4. Conclusions

The analysis of a 14-member ensemble in terms of simulation skills showed a better performance in replicating the climatologic intra-regional variability of annual temperature in the SA for two RCMs (CCLM4-8-17 and RCA4) nested in HadGEM2-ES. This complies with the findings by Aziz et al. (2020), who showed the better skill of two models in reproducing mean daily temperature climatology regarding the regional averages for the Mediterranean, Aegean, and Central Anatolia regions of Turkey. In our study, two high-resolution MRI climate models, NHRCM nested in MRI-AGCM and MRI-AGCM without downscaling, also show high simulation skills. However, it should be noted that among the driving GCMs used in this study, MRI-AGCM uses prescribed observation-based SST that eliminates potential biases in SST, unlike other CMIP5 GCMs.

The RCMs using EC-EARTH as the driving model show varying performance skills for temperature, while CNRM-CM5 as the driving model produced a relatively poor performance for the SA. For RCMs with CM5A-MR forcing, simulation performances are found not to be either significantly strong or weak relative to other models, although according to the analysis by McSweeney et al. (2015), CM5A-MR exhibited poor performance, especially concerning its ability to accurately replicate the annual cycles of temperature and precipitation in the Mediterranean region. Regarding other driving GCMs in our study, McSweeney et al. (2015) also found that CNRM-CM5, EC-EARTH, and HadGEM2-ES are satisfactory for the simulation in the EURO domain regarding the reproduction of the circulation patterns, storm tracks, and the annual temperature and precipitation cycles. Nevertheless, the poor performance of CNRM-CM5 as driving GCM for the simulation of $\overline{T_{annual}}$ in the SA is interpreted to be connected to the technical problem in the model related to the boundary forcing conditions (EURO-CORDEX, 2021). Furthermore, unlike other driving GCMs in this study, CNRM-CM5 does not include forcing for land-use change (Collins et al., 2013; Boé et al.,

2020), which may be another factor for its relatively weak performance, particularly considering that none of the CORDEX RCMs in this study includes forcing of land cover changes (Boé et al., 2020). Similar uncertainties in CORDEX are confirmed by Ito et al. (2020).

The analysis of ΔT_{annual} for the short-, medium-, and long-term projections demonstrated a statistically significant temperature increase by the end of the current century for the entire SA and all three future projections under both moderate (RCP4.5) and high (RCP8.5) CO_2 emission scenarios. For both projections conditions and in all three future scenarios RACMO22E, RCA4, WRF331F, ALADIN53, MRI-AGCM, and NHRCM are seen to project a more pronounced increase in annual temperature for inland parts of the SA compared to the coastal parts. This is considered to be connected with the influence of the Mediterranean and Aegean seas and the dry climate in inland regions, which is most pronounced in the Central Anatolia region with low annual mean precipitation (< 1 mm d^{-1}) (Mesta et al., 2022).

All models in the 14-member ensemble agree on a gradual and statistically significant increase in temperature under both RCP4.5 and RCP8.5 scenarios across the entire SA. Under RCP4.5, most of the models indicate a decline in the rate of increase in temperature (increase per decade) for the long term in the second half of the century, whereas, under RCP8.5, the models mostly show a relatively higher rate of increase for the long-term period compared to the medium-term period.

Averaging the results from the 12 CORDEX RCMs under the RCP4.5 scenario, a likely increase in the areal average of $\overline{T_{annual}}$ is projected for the entire SA as 1.2, 1.6, and 2.5 ºC for short-, medium- and long-term scenarios, respectively. The likely increase in ΔT_{annual} under RCP8.5 is 1.4, 2.1, and 4.1 ºC for the short-, medium-, and long-term scenarios, respectively. Additionally, MRI's MRI-AGCM, and NHRCM project a 4.9 and 4.7 ºC increase in $\overline{T_{annual}}$ in the study area for a 20-year period at the end of the 21st century.

A combined analysis of the projections on the percent temperature increase and percent decrease in precipitation in the SA basins supports an inverse linear relationship. Hence, climate change is expected to amplify drought, particularly in inland basins with increased temperatures due to the prevailing dry climate.

From the findings of the study:

- The analysis reveals significant variability in the simulation capabilities of 14 climate models concerning the spatial distribution of $\overline{T_{annual}}$ within the SA.
- The multi-model ensemble analysis verifies a gradual increase in the temperature by 2100 under both RCP4.5 and RCP8.5 scenarios in the entire study area.
- Under the RCP4.5 scenario, most models in the ensemble agree that the warming will continue, although the rate of increase is expected to diminish. For the RCP8.5 scenario, the projections mostly agree on an increase with an even more elevated rate in the latter half of the 21st century.
- The temperature increase in the inland basins is likely to be more pronounced than in the coastal areas, which is interpreted to be connected to the drying effect of climate change.
- The simultaneous decrease in precipitation with the increase in temperature at all basins in the SA is expected to aggravate the impacts on water resources in the SA, which necessitates tiered adaptation measures to be put into use.

This study focuses on seasonal mean climatologies. Practical adaptations to the future changes in surface air temperatures require more fine temporal resolutions, such as hourly time scales, because heat fluxes and evaporations are controlled by diurnal cycles of surface air temperatures. Therefore, in a future study, a convection-permitting model with a spatial resolution of 2 km or less is required to simulate the diurnal cycles and to project the changes (Pinzón et al., 2021; Takayabu et al., 2021).

Acknowledgments

The authors express their gratitude to the Scientific and Technological Research Council of Turkey (TÜBİTAK) and the Japan Society for the Promotion of Science (JSPS), grant number JPJSBP12019940, for their invaluable support in facilitating this collaborative research effort. The creation of NHRCM simulations was further made possible through backing from the

Integrated Research Program for Advancing Climate Models (TOUGOU), grant number JPMXD0717935561, and advanced studies on climate change projection (SENTAN), grant number JPMXD0722680734, from the Ministry of Education, Culture, Sports, Science, and Technology (MEXT) of Japan. Additionally, this research is financially supported by the Scientific and Technological Research Council of Turkey (TÜBİTAK) under the project titled "Assessment of climate change impacts on streamflow and hydropower in Antalya, Turkey", grant number 118Y365.

References

Acar Deniz Z, Gönençgil B. 2015. Trends of summer daily maximum temperature extremes in Turkey. Physical Geography 36: 268-281. https://doi.org/10.1080/02723646.2015.1045285

Aziz R, Yucel I, Yozgatligil C. 2020. Nonstationarity impacts on frequency analysis of yearly and seasonal extreme temperature in Turkey. Atmospheric Research 238: 104875. https://doi.org/10.1016/j.atmosres.2020.104875

Bağçaci SÇ, Yucel I, Duzenli E, Yilmaz MT. 2021. Intercomparison of the expected change in the temperature and the precipitation retrieved from CMIP6 and CMIP5 climate projections: A Mediterranean hot spot case, Turkey. Atmospheric Research 256:105576. https://doi.org/10.1016/j.atmosres.2021.105576

Bartolini G, Di Stefano V, Maracchi G, Orlandini S. 2012. Mediterranean warming is especially due to summer season. Theoretical and Applied Climatology 107: 279-295. https://doi.org/10.1007/s00704-011-0481-1

Bayer Altın T, Barak B. 2017. Trends and changes in tropical and summer days at the Adana sub-region of the Mediterranean region, southern Turkey. Atmospheric Research 196: 182-199. https://doi.org/10.1016/j.atmosres.2017.06.017

Beck HE, Zimmermann NE, McVicar TR, Vergopolan N, Berg A, Wood EF. 2018. Present and future Köppen-Geiger climate classification maps at 1-km resolution. Scientific Data 5: 180214. https://doi.org/10.1038/sdata.2018.214

Boé J, Somot S, Corre L, Nabat P. 2020. Large discrepancies in summer climate change over Europe as projected by global and regional climate models: Causes and consequences. Climate Dynamics 54: 2981-3002. https://doi.org/10.1007/s00382-020-05153-1

Bøssing Christensen O, Drews M, Hesselbjerg Christensen J, Dethloff K, Ketelsen K, Hebestadt I, Rinke A. 2007. The HIRHAM regional climate model, v. 5 (beta). Technical Report No. 06-17. Danish Meteorological Institute, Denmark.

Byrne MP, O'Gorman PA. 2018. Trends in continental temperature and humidity directly linked to ocean warming. Proceedings of the National Academy of Sciences 115: 4863-4868. https://doi.org/10.1073/pnas.1722312115

Cagatan K, Unal Y. 2010. Heat wave tendency in the western part of Turkey and its relation to circulation patterns. In: EGU General Assembly Conference Abstracts, vol. 12, EGU2010-8507.

Colin J, Déqué M, Radu R, Somot S. 2010. Sensitivity study of heavy precipitations in limited area model climate simulation: Influence of the size of the domain and the use of the spectral nudging technique. Tellus A: Dynamic Meteorology and Oceonography 62: 591-604. https://doi.org/10.1111/j.1600-0870.2010.00467.x

Collins M., Knutti R, Arblaster J, Dufresne J-L, Fichefet T, Friedlingstein P, Gao X, Gutowski WJ, Johns T, Krinner G, Shongwe M, Tebaldi C, Weaver AJ, Wehner M. 2013: Long-term Climate Change: Projections, Commitments and Irreversibility. In: Climate Change 2013: The Physical Science Basis. Contribution of Working Group I to the Fifth Assessment Report of the Intergovernmental Panel on Climate Change [Stocker TF, Qin D, Plattner G-K, Tignor M, Allen SK, Boschung J, Nauels A, Xia Y, Bex V, Midgley PM (eds.)]. Cambridge University Press, Cambridge, United Kingdom and New York, , 1029-1136. https://doi.org/10.1017/CBO9781107415324.024

EEA-JRC. 2012. Copernicus Land Monitoring Service (CLMS). CORINE Land Cover CCL 2012 website. European Environment Agency and the Joint Research Centre. Available at https://land.copernicus.eu/pan-european/corine-land-cover/clc-2012 (accessed 2018 January 7).

Efthymiadis D, Goodess CM, Jones PD. 2011. Trends in Mediterranean gridded temperature extremes and large-scale circulation influences. Natural Hazards and Earth System Sciences 11: 2199-2214. https://doi.org/10.5194/nhess-11-2199-2011

Erlat E, Türkeş M, Aydin-Kandemir F. 2021. Observed changes and trends in heatwave characteristics in Turkey since 1950. Theoretical and Applied Climatology 145: 137-157. https://doi.org/10.1007/s00704-021-03620-1

ESGF. 2021. CORDEX Database. CoG v. v4.0.0b2, ESGF P2P v. v4.0.4. Earth System Grid Federation (ESGF) website. Available at https://esgf-node.llnl.gov/search/esgf-llnl/ (accessed 2021 December 21)

EURO-CORDEX. 2021. EURO-CORDEX errata page, errata table. Available at https://www.euro-cordex.net/078730/index.php.en (accessed 2021 December 21)

Giorgi F. 2006. Climate change hot-spots. Geophysical Research Letters 33: L08707. https://doi.org/10.1029/2006GL025734

Giorgi F, Lionello P. 2008. Climate change projections for the Mediterranean region. Global and Planetary Change 63: 90-104. https://doi.org/10.1016/j.gloplacha.2007.09.005

Gönençgil B, Acar Denis Z. 2016. Extreme maximum and minimum air temperature in Mediterranean coasts in Turkey. Geography, Environment, Sustainability 9: 59-70. https://doi.org/10.15356/2071-9388_01v09_2016_05

Gutiérrez C, Somot S, Nabat P, Mallet M, Corre L, van Meijgaard E, Perpiñán O, Gaertner MÁ. 2020. Future evolution of surface solar radiation and photovoltaic potential in Europe: Investigating the role of aerosols. Environmental Research Letters 15: 034035. https://doi.org/10.1088/1748-9326/ab6666

Haarsma RJ, Selten F, Hurk BV, Hazeleger W, Wang X. 2009. Drier Mediterranean soils due to greenhouse warming bring easterly winds over summertime central Europe. Geophysical Research Letters 36: L04705. https://doi.org/10.1029/2008GL036617

IPCC. 2021. Climate Change 2021: The Physical Science Basis (Masson-Delmotte V, Zhai P, Pirani A, Connors SL, Péan C, Berger S, Caud N, Chen Y, Goldfarb L, Gomis MI, Huang M, Leitzell K, Lonnoy E, Matthews JBR, Maycock TK, Waterfield T, Yelekçi O, Yu R, Zhou B., Eds.). Contribution of Working Group I to the Sixth Assessment Report of the Intergovernmental Panel on Climate Change. Cambridge and New York, Cambridge University Press, 2391 pp. https://doi.org/10.1017/9781009157896

Ito R, Shiogama H, Nakaegawa T, Takayabu I. 2020. Uncertainties in climate change projections covered by the ISIMIP and CORDEX model subsets from CMIP5. Geoscientific Model Development 13: 859-872. https://doi.org/10.5194/gmd-13-859-2020

Jerez S, Lopez-Romero JM, Turco M, Jiménez-Guerrero P, Vautard R, Montavez JP. 2018. Impact of evolving greenhouse gas forcing on the warming signal in regional climate model experiments. Nature Communications 9: 1304. https://doi.org/10.1038/s41467-018-03527-y

Karadag H, Yildiz K, Yürekli K. 2023. Historical change of winter chill accumulation in some regions of Turkey. Atmósfera 37: 285-294. https://doi.org/10.20937/ATM.53135

Kjellström E, Bärring L, Nikulin G, Nilsson C, Persson G, Strandberg G. 2016. Production and use of regional climate model projections – A Swedish perspective on building climate services. Climate Services 2-3: 15-29. https://doi.org/10.1016/j.cliser.2016.06.004

Kostopoulou E, Jones PD. 2005. Assessment of climate extremes in the Eastern Mediterranean. Meteorology and Atmospheric Physics 89: 69-85. https://doi.org/10.1007/s00703-005-0122-2

Kuglitsch FG, Toreti A, Xoplaki E, Della-Marta PM, Zerefos CS, Türkeş M, Luterbacher J. 2010. Heat wave changes in the eastern Mediterranean since 1960. Geophysical Research Letters 37: L04802. https://doi.org/10.1029/2009GL041841

Kurtzman D, Kadmon R. 1999. Mapping of temperature variables in Israel: SA comparison of different interpolation methods. Climate Research 13: 33-43. https://doi.org/10.3354/cr013033

Kusunoki S, Nakaegawa T, Pinzón R, Sánchez-Galán JE, Fábrega JR. 2019. Future precipitation changes over Panama projected with the atmospheric global model MRI-AGCM3.2. Climate Dynamics 53: 5019-5034. https://doi.org/10.1007/s00382-019-04842-w

Lionello P, Malanotte-Rizzoli P, Boscolo R, Alpert P, Artale V, Li L, Luterbacher J, May W, Trigo R, Tsimplis M, Ulbrich U, Xoplaki E. 2006. The Mediterranean climate: An overview of the main characteristics and issues. In: Mediterranean (Lionello P, Malanotte-Rizzoli P, Boscolo R, Eds.). Developments in Earth and environmental sciences, vol. IV, Elsevier, 1-41. https://doi.org/10.1016/S1571-9197(06)80003-0

Mahmood R, Pielke RA, Hubbard KG, Niyogi D, Bonan G, Lawrence P, McNider R, McAlpine C, Etter A, Gameda S, Qian B, Carleton A, Beltran-Przekurat A, Chase T, Quintanar AI, Adegoke JO, Vezhapparambu S, Conner G, Asefi S, Sertel E, Legates DR, Wu Y, Hale R, Frauenfeld OW, Watts A, Shepherd M, Mitra C, Anantharaj VG, Fall S, Lund R, Treviño A, Blanken P, Du J, Chang HI, Leeper R, Nair US, Dobler S, Deo R, Syktus J. 2010. Impacts of land use/land cover change on climate and future research priorities. Bulletin of the

American Meteorological Society 91: 37-46. https://doi.org/10.1175/2009BAMS2769.1

McSweeney CF, Jones RG, Lee RW, Rowell DP. 2015. Selecting CMIP5 GCMs for downscaling over multiple regions. Climate Dynamics 44: 3237-3260. https://doi.org/10.1007/s00382-014-2418-8

Mesta B, Kentel E. 2021. Superensembles of raw and bias-adjusted regional climate models for Mediterranean region, Turkey. International Journal of Climatology 42: 2566-2585. https://doi.org/10.1002/joc.7381

Mesta B. 2022. Impact of climate change in the southern Mediterranean of Turkey: A method to assess Oymapinar reservoir's inflow projections. Ph.D. thesis, Middle East Technical University, Ankara, Turkey.

Mesta B, Sasaki H, Nakaegawa T, Kentel E. 2022. Changes in precipitation climatology for the Eastern Mediterranean using CORDEX RCMs, NHRCM and MRI-AGCM. Atmospheric Research 272: 106140. https://doi.org/10.1016/j.atmosres.2022.106140

Mizuta R, Oouchi K, Yoshimura H, Noda A, Katayama K, Yukimoto S, Hosaka M, Kusunoki S, Kawai H, Nakagawa M. 2006. 20-km-mesh global climate simulations using JMA-GSM model – Mean climate states. Journal of the Meteorological Society of Japan Ser. II 84: 165-185. https://doi.org/10.2151/jmsj.84.165

Nakaegawa T, Kitoh A, Kusunoki S, Murakami H, Arakawa O. 2014. Hydroclimate change over Central America and the Caribbean in a global warming climate projected with 20-km and 60-km mesh MRI atmospheric general circulation models. Papers in Meteorology and Geophysics 65: 15-33. https://doi.org/10.2467/mripapers.65.15

Nakaegawa T, Hibino K, Takayabu I. 2017. Identifying climate analogues for cities in Australia by a non-parametric approach using multi-ensemble, high-horizontal resolution future climate projections by an atmospheric general circulation model, MRI-AGCM3.2H. Hydrological Research Letters 11: 72-78. https://doi.org/10.3178/hrl.11.72

Önol B, Unal YS. 2014. Assessment of climate change simulations over climate zones of Turkey. Regional Environmental Change 14: 1921-1935. https://doi.org/10.1007/s10113-012-0335-0

Öztürk T, Ceber ZP, Türkeş M, Kurnaz ML. 2015. Projections of climate change in the Mediterranean Basin by using downscaled global climate model outputs. International Journal of Climatology 35: 4276-4292. https://doi.org/10.1002/joc.4285

Pinzón R, Ishizaki NN, Sasaki H, Nakaegawa T. 2021. Panama's current climate replicability in a non-hydrostatic regional climate model nested in an atmospheric general circulation model. Atmosphere 12: 1543. https://doi.org/10.3390/atmos12121543

Rockel B, Will A, Hense A. 2008. The regional climate modelling with COSMO-CLM (CCLM). Meteorologische Zeitschrift 17: 347-348. https://doi.org/10.1127/0941-2948/2008/0309

Sakalis VD. 2024. Trend analysis and forecast of annual precipitation and temperature series in the Eastern Mediterranean region. Atmósfera 38: 381-408. https://doi.org/10.20937/ATM.53272

Sasaki H, Kurihara K. 2008. Relationship between precipitation and elevation in the present climate reproduced by the non-hydrostatic regional climate model. Scientific Online Letters on the Atmosphere (SOLA) 4: 109-112. https://doi.org/10.2151/sola.2008-028

Sasaki H, Kurihara K, Takayabu I, Uchiyama T. 2008. Preliminary experiments of reproducing the present climate using the non-hydrostatic regional climate model. Scientific Online Letters on the Atmosphere (SOLA) 4: 025-028. https://doi.org/10.2151/sola.2008-007

Sasaki H, Murata A, Hanafusa M, Oh'izumi M, Kurihara K. 2011. Reproducibility of present climate in a non-hydrostatic regional climate model nested within an atmosphere general circulation model. Scientific Online Letters on the Atmosphere (SOLA) 7: 173-176. https://doi.org/10.2151/sola.2011-044

Sasaki H, Murata A, Hanafusa M, Oh'izumi M, Kurihara K. 2012. Projection of future climate change in a non-hydrostatic regional climate model nested within an atmospheric general circulation model. Scientific Online Letters on the Atmosphere (SOLA) 8: 53-56. https://doi.org/10.2151/sola.2012-014

Sasaki H, Kurihara K, Murata A, Hanafusa M, Oh'izumi M. 2013. Future changes of snow depth in a non-hydrostatic regional climate model with bias correction. Scientific Online Letters on the Atmosphere (SOLA) 9: 5-8. https://doi.org/10.2151/sola.2013-002

Selten FM, Bintanja R, Vautard R, van den Hurk BJJM. 2020. Future continental summer warming constrained by the present-day seasonal cycle of surface hydrology. Scientific Reports 10: 4721. https://doi.org/10.1038/s41598-020-61721-9

Seneviratne SI, Corti T, Davin EL, Hirschi M, Jaeger EB, Lehner I, Orlowsky B, Teuling AJ. 2010. Investigating

soil moisture-climate interactions in a changing climate: A review. Earth-Science Reviews 99: 125-161. https://doi.org/10.1016/j.earscirev.2010.02.004

Seneviratne SI, Wilhelm M, Stanelle T, van den Hurk B, Hagemann S, Berg A, Cheruy F, Higgins ME, Meier A, Brovkin V, Claussen M, Ducharne A, Dufresne JL, Findell KL, Ghattas J, Lawrence DM, Malyshev S, Rummukainen M, Smith B. 2013. Impact of soil moisture-climate feedbacks on CMIP5 projections: First results from the GLACE-CMIP5 experiment. Geophysical Research Letters 40: 5212-5217. https://doi.org/10.1002/grl.50956

Sensoy S, Demircan M, Ulupınar Y. 2016. Climate of Turkey. Turkish State Meteorological Service, Ankara, Turkey. Available at https://www.researchgate.net/publication/296597022_Climate_of_Turkey. (accessed 2021 December 21)

Setianto A, Triandini T. 2013. Comparison of kriging and inverse distance weighted (IDW) interpolation methods in lineament extraction and analysis. Journal of Applied Geology 5: 21-29. https://doi.org/10.22146/jag.7204

Skamarock WC, Klemp JB, Dudhia J, Gill DO, Baker DM, Duda MG, Huang XY, Wang W, Powers JG. 2008. A description of the advanced research WRF v. 3. NCAR/TN-475 NCAR Technical Note. National Centre for Atmospheric Research, Boulder, Colorado, USA. https://doi.org/10.5065/D68S4MVH

Sørland SL, Fischer AM, Kotlarski S, Künsch HR, Liniger MA, Rajczak J, Schär C, Spirig C, Strassmann K, Knutti R. 2020. CH2018 – National climate scenarios for Switzerland: How to construct consistent multi-model projections from ensembles of opportunity. Climate Services 20: 100196. https://doi.org/10.1016/j.cliser.2020.100196

Takayabu I, Ishizaki NN, Nakaegawa T, Sasaki H, Wongseree W. 2021. Potential of representing the diurnal cycle of local-scale precipitation in northeastern Thailand using 5-km and 2-km grid regional climate models. Hydrological Research Letters 15: 1-8. https://doi.org/10.3178/hrl.15.1

Tanarhte M, Hadjinicolaou P, Lelieveld J. 2015. Heat wave characteristics in the eastern Mediterranean and Middle East using extreme value theory. Climate Research 63: 99-113. https://doi.org/10.3354/cr01285

Tayanç M, İm U, Doğruel M, Karaca M. 2009. Climate change in Turkey for the last half century. Climatic Change 94: 483-502. https://doi.org/10.1007/s10584-008-9511-0

Toros H. 2011. Spatio-temporal variation of daily extreme temperatures over Turkey. International Journal of Climatology 32: 1047-1055. https://doi.org/1047-1055.10.1002/joc.2325

Unal YS, Tan E, Mentes SS. 2013. Summer heat waves over western Turkey between 1965 and 2006. Theoretical and Applied Climatology 112: 339-350. https://doi.org/10.1007/s00704-012-0704-0

Van Meijgaard E, Van Ulft LH, Lenderink SG, de Roode SR, Wipfler L, Boers R, Timmermans RMA. 2012. Refinement and application of a regional atmospheric model for climate scenario calculations of Western Europe. KVR report 054/12. The Royal Netherlands Meteorological Institute, 44 pp.

Yang W, Zhao Y, Wang D, Wu H, Lin A, He L. 2020. Using principal components analysis and IDW interpolation to determine spatial and temporal changes of surface water quality of Xin'anjiang river in Huangshan, China. International Journal of Environmental Research and Public Health 17: 2942. https://doi.org/10.3390/ijerph17082942

Zampieri M, D'andrea F, Vautard R, Ciais P, de Noblet-Ducoudré N, Yiou P. 2009. Hot European summers and the role of soil moisture in the propagation of Mediterranean drought. Journal of Climate 22: 4747-4758. https://doi.org/10.1175/2009JCLI2568.1

Zittis G, Hadjinicolaou P, Lelieveld J. 2014. Role of soil moisture in the amplification of climate warming in the eastern Mediterranean and the Middle East. Climate Research 59: 27-37. https://doi.org/10.3354/cr01205

Zittis G, Hadjinicolaou P. 2016. The effect of radiation parameterization schemes on surface temperature in regional climate simulations over the MENA-CORDEX domain. International Journal of Climatology 37: 3847-3862. https://doi.org/10.1002/joc.4959

Supplementary Material

S1. Meteorological stations and major hydrological basins in the study area

Table SI. Stations and station IDs.

Station ID	Station name	Latitudes (DD)	Longitudes (DD)	Elevation (masl)	Station ID	Station Name	Latitudes (DD)	Longitudes (DD)	Elevation (masl)
5643*	Suhut	38.53	30.55	1130	17375	Finike	36.30	30.15	2
17826*	Senirkent	38.10	30.56	959	17380	Kas	36.20	29.65	153
6679	Atabey KK	37.95	30.65	1000	17748	Simav	39.09	28.98	809
7538	Bucak	37.47	30.58	850	17750	Gediz	38.99	29.40	736
8229	Akseki	37.05	31.78	1150	17752	Emirdag	39.01	31.15	983
8355	Buk O.A.	36.93	30.45	475	17754	Kulu	39.08	33.07	1005
9022	Tarsus K.H.	36.92	34.90	11	17796	Bolvadin	38.73	31.05	1018
17188	Usak	38.67	29.40	919	17798	Yunak	38.82	31.73	1148
17190	Afyon	38.74	30.56	1034	17824	Guney	38.15	29.06	825
17191	Cihanbeyli	38.65	32.92	973	17828	Yalvac	38.28	31.18	1096
17192	Aksaray	38.37	34.00	970	17832	Ilgin	38.28	31.89	1036
17237	Denizli	37.76	29.09	425	17862	Dinar	38.06	30.15	864
17238	Burdur	37.72	30.29	957	17864	Uluborlu	38.09	30.46	1025
17239	Aksehir	38.37	31.43	1002	17882	Egirdir	37.84	30.87	920
17240	Isparta	37.78	30.57	997	17884	Milas	37.30	27.78	57
17242	Beysehir	37.68	31.75	1141	17886	Yatagan	37.34	28.14	365
17244	Konya Airport	37.98	32.57	1031	17890	Acipayam	37.43	29.35	941
17246	Karaman	37.19	33.22	1018	17892	Tefenni	37.32	29.78	1142
17248	Eregli	37.53	34.05	1046	17898	Seydisehir	37.43	31.85	1129
17290	Bodrum	37.03	27.44	26	17900	Cumra	37.57	32.79	1014
17292	Mugla	37.21	28.37	646	17902	Karapinar	37.71	33.53	996
17294	Dalaman	36.77	28.80	12	17924	Koycegiz	36.97	28.69	24
17296	Fethiye	36.63	29.12	3	17926	Korkuteli	37.06	30.19	1017
17297	Datca	36.71	27.69	28	17928	Hadim	36.99	32.46	1552
17298	Marmaris	36.84	28.25	16	17952	Elmali	36.74	29.91	1095
17300	Antalya Airport	36.91	30.80	64	17954	Manavgat	36.79	31.44	38
17310	Alanya	36.55	31.98	6	17956	Mut	36.65	33.43	340
17320	Anamur	36.07	32.86	2	17958	Erdemli	36.63	34.34	7
17330	Silifke	36.38	33.94	10	17974	Gazipasa	36.27	32.30	21
17340	Mersin	36.78	34.60	7					

DD: decimal degrees.
*Represented by the same model grid.

Table SII. List of basins in the study area.

basin name
Middle Mediterranean (Antalya) basin
Western Mediterranean basin
Eastern Mediterranean basin
Konya Closed basin
Akarcay basin
B. Menderes basin
Burdur basin
Gediz basin
Sakarya basin
Susurluk basin

S2. Analysis of simulation skills of climate models for spatial variability of seasonal temperature climatology

Table SIII. Performance indicator values for climate models regarding the spatial variability of the seasonal climatology.

	DJF			MAM			JJA			SON		
	Corr	Bias* (ºC)	RMSE (ºC)	Corr	Bias* (ºC)	RMSE (ºC)	Corr	Bias* (ºC)	RMSE (ºC)	Corr	Bias* (ºC)	RMSE (ºC)
M1	0.91	–0.98	2.06	0.89	–1.02	1.86	0.80	1.01	**1.99**	0.89	**0.08**	**1.70**
M2	0.91	**–0.58**	**1.89**	0.90	**0.45**	**1.39**	0.82	1.90	2.40	0.90	0.75	1.74
M3	0.88	–5.16	43.4	0.87	–4.80	40.57	0.83	–3.18	30.0	0.85	–4.44	38.6
M4	0.94	–2.46	22.2	0.92	–2.48	22.04	0.85	–3.31	28.7	0.92	–2.31	21.3
M5	0.95	–2.48	21.8	0.93	–3.37	27.64	0.87	–2.60	23.5	0.92	–2.65	23.1
M6	0.95	–2.56	22.7	0.92	–2.30	20.69	0.86	–2.64	23.2	0.93	–3.00	25.6
M7	0.94	–0.81	14.1	0.90	–1.03	14.06	0.86	–2.22	21.1	0.92	–2.28	21.7
M8	0.95	–4.94	41.2	0.93	–4.70	38.87	0.88	–3.28	27.2	0.93	–3.77	31.0
M9	0.96	–3.18	26.4	0.94	–3.78	30.73	0.88	–2.95	24.9	**0.94**	–3.77	30.7
M10	0.94	–2.39	21.5	0.92	–3.18	26.37	**0.91**	–1.69	16.5	0.93	–2.64	22.6
M11	0.92	–2.25	21.9	0.90	–3.81	31.57	0.87	–2.27	20.6	0.90	–1.94	19.1
M12	0.94	–2.02	19.5	0.91	–1.54	16.29	0.78	**–0.22**	12.6	0.91	–1.21	15.3
M13	**0.96**	–4.10	35.0	0.94	–3.77	32.97	0.90	–1.21	13.9	0.93	–2.11	20.1
M14	0.95	–1.92	18.0	**0.94**	–2.53	22.02	0.89	–1.16	14.0	0.93	–2.14	19.8

*Mean difference between observed and simulated.
Corr: Pearson's correlation coefficient; RMSE: root mean square error.
Best values are indicated in bold.¡

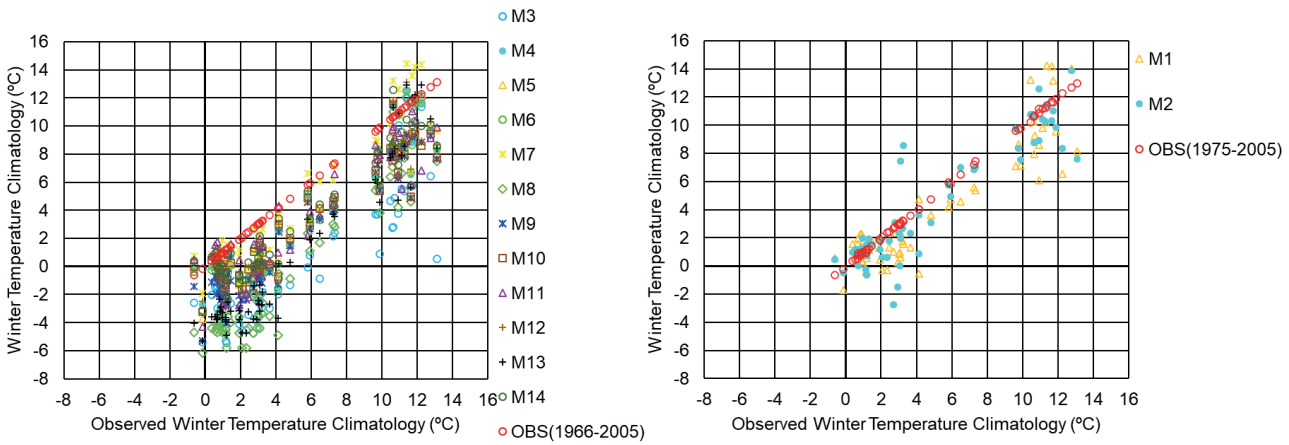

Fig. S1. Comparison between observed and modeled seasonal temperature climatology for winter (DJF).

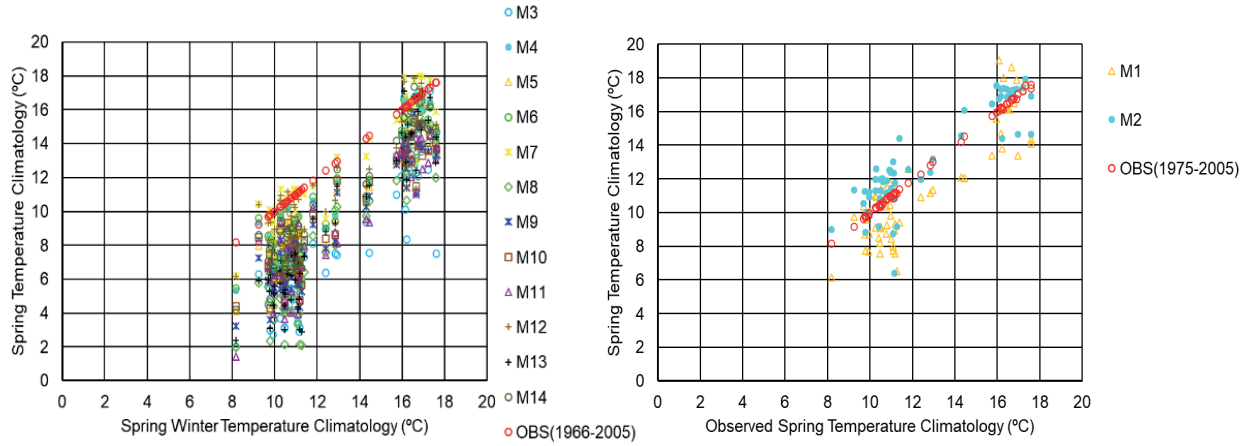

Fig. S2. Comparison between observed and modeled seasonal temperature climatology for Spring (MAM).

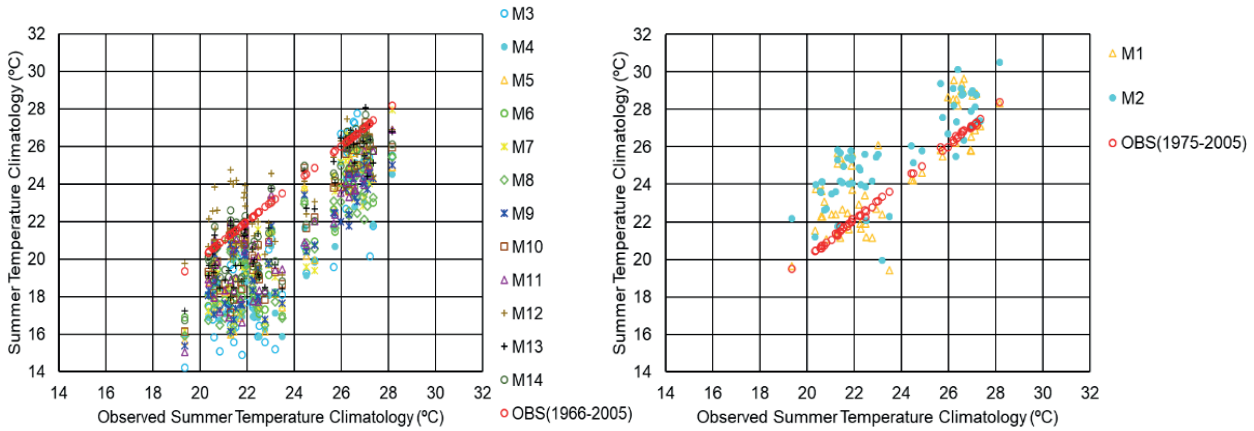

Fig. S3. Comparison between observed and modeled seasonal temperature climatology for summer (JJA).

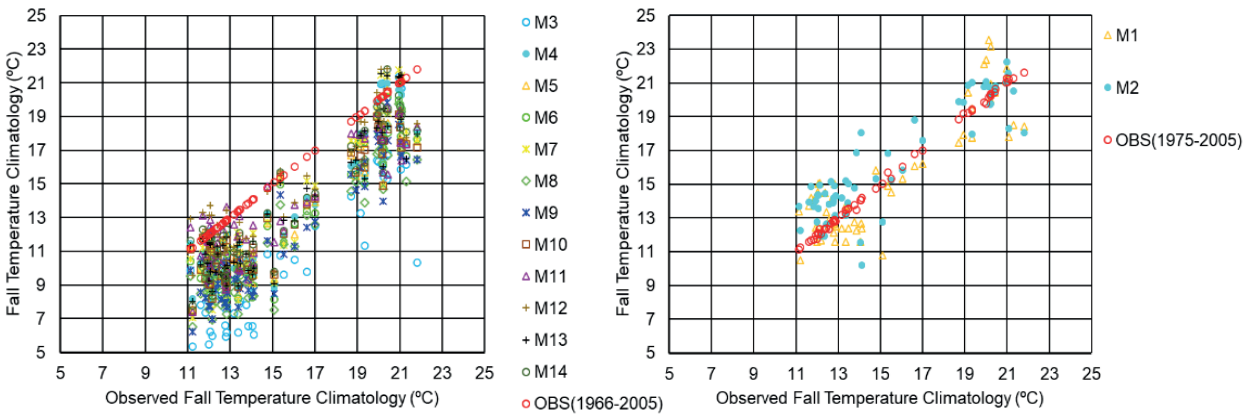

Fig. S4. Comparison between observed and modeled seasonal temperature climatology for fall (SON).

S.3 Short-, medium-, and long- term projections from CORDEX models for temperature change under RCP 4.5 and RCP8.5 scenarios (ΔTannual [ºC])

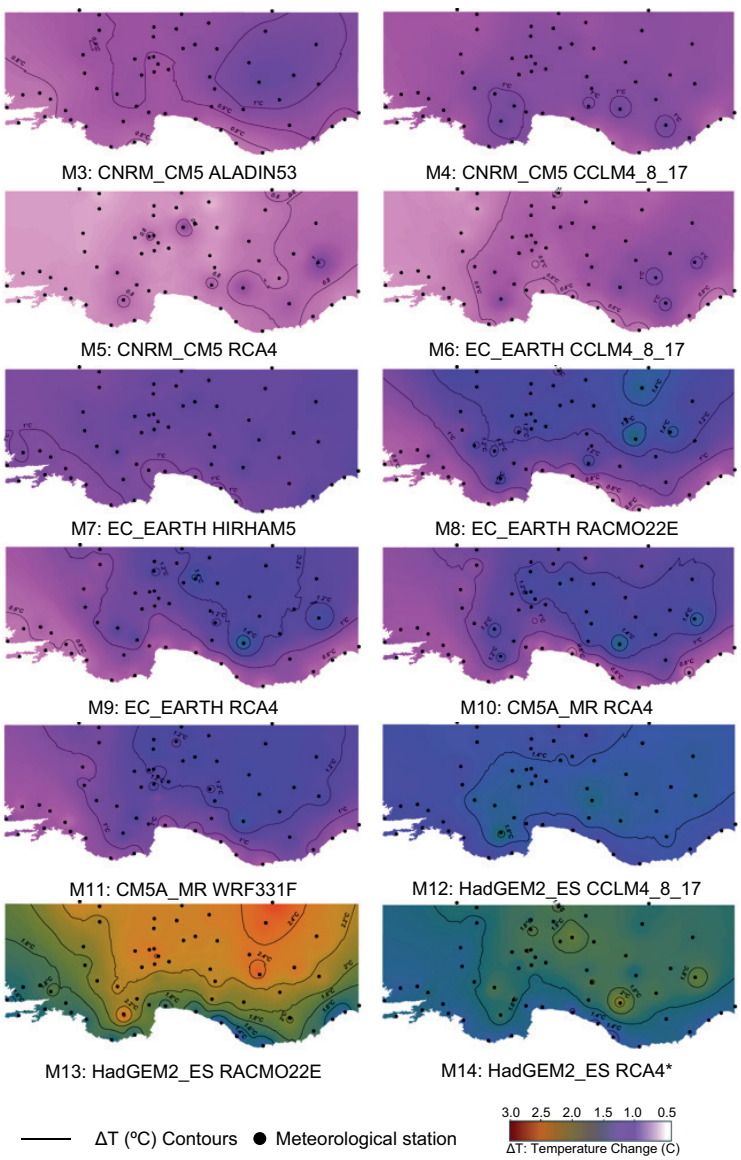

Fig. S7. Short-term temperature change projections (RCP4.5) (ΔT_{annual} [ºC]) for models M3 through M14. All changes are verified to be statistically significant at the 95% confidence level. (*Best performing CORDEX model for the study area).

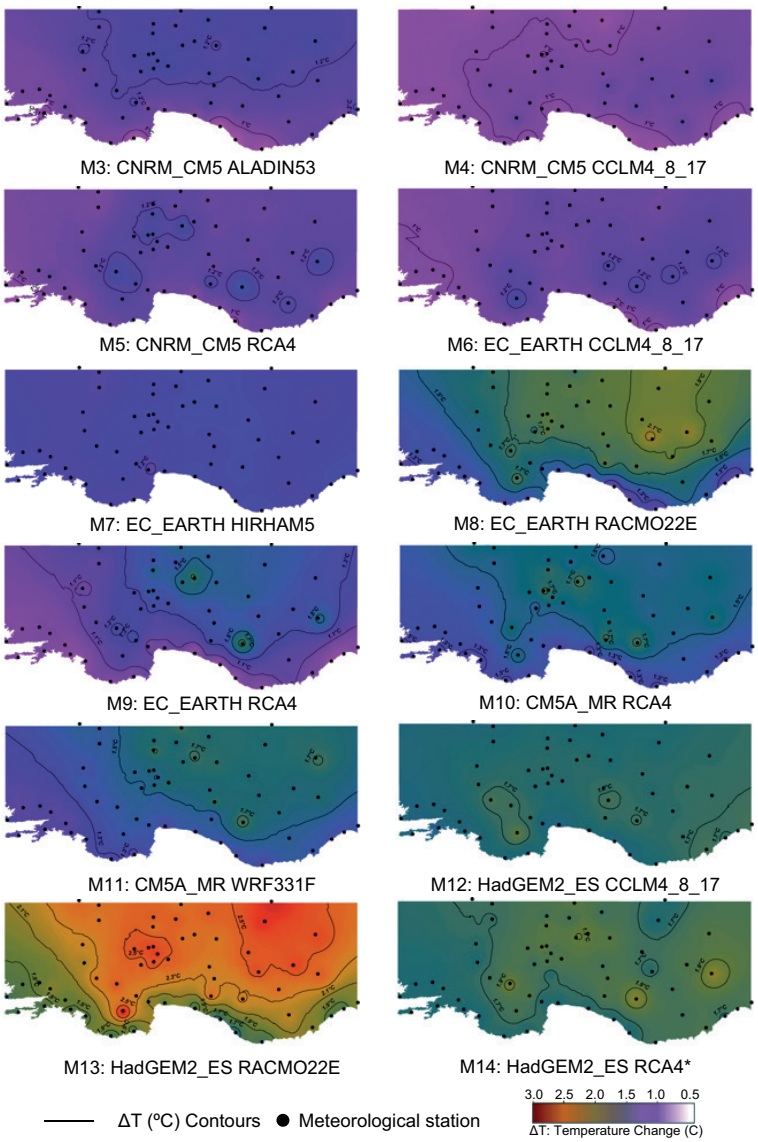

Fig. S8. Short-term temperature change projections (RCP8.5) (ΔT_{annual} [ºC]) for models M3 through M14. All changes are verified to be statistically significant at the 95% confidence level. (*Best performing CORDEX model for the study area).

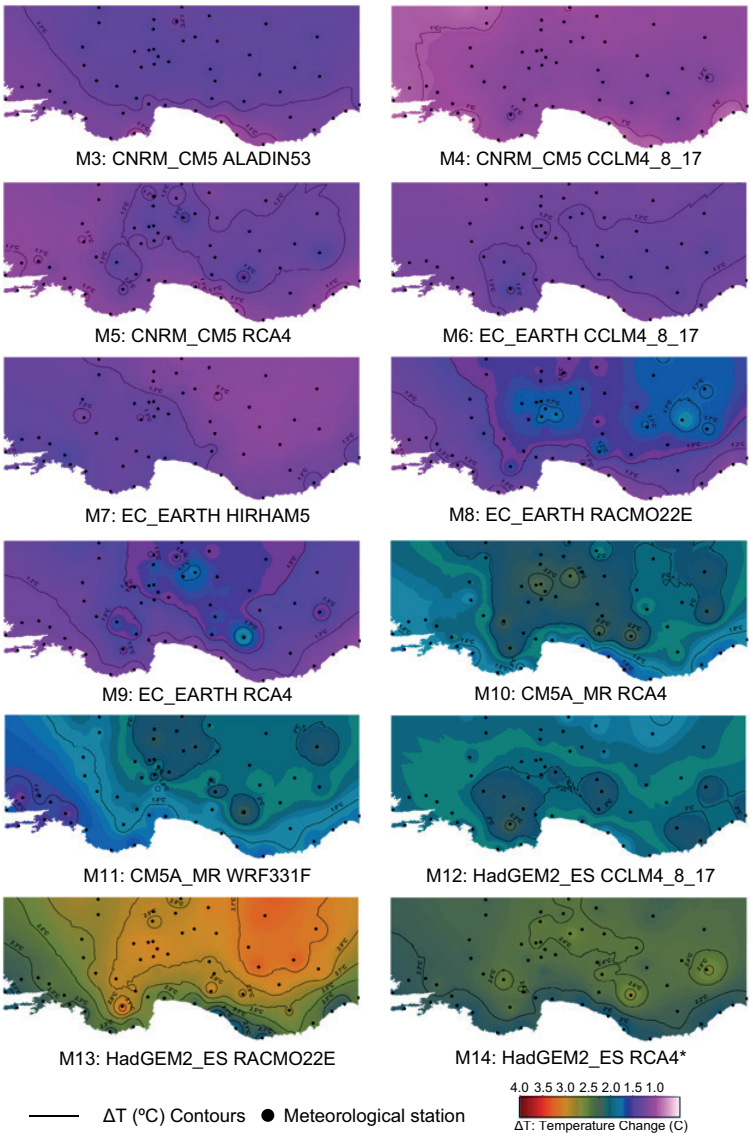

Fig. S9. Medium-term temperature change projections (RCP4.5) (ΔT_{annual} [ºC]) for models M3 through M14. All changes are verified to be statistically significant at the 95% confidence level. (*Best performing CORDEX model for the study area).

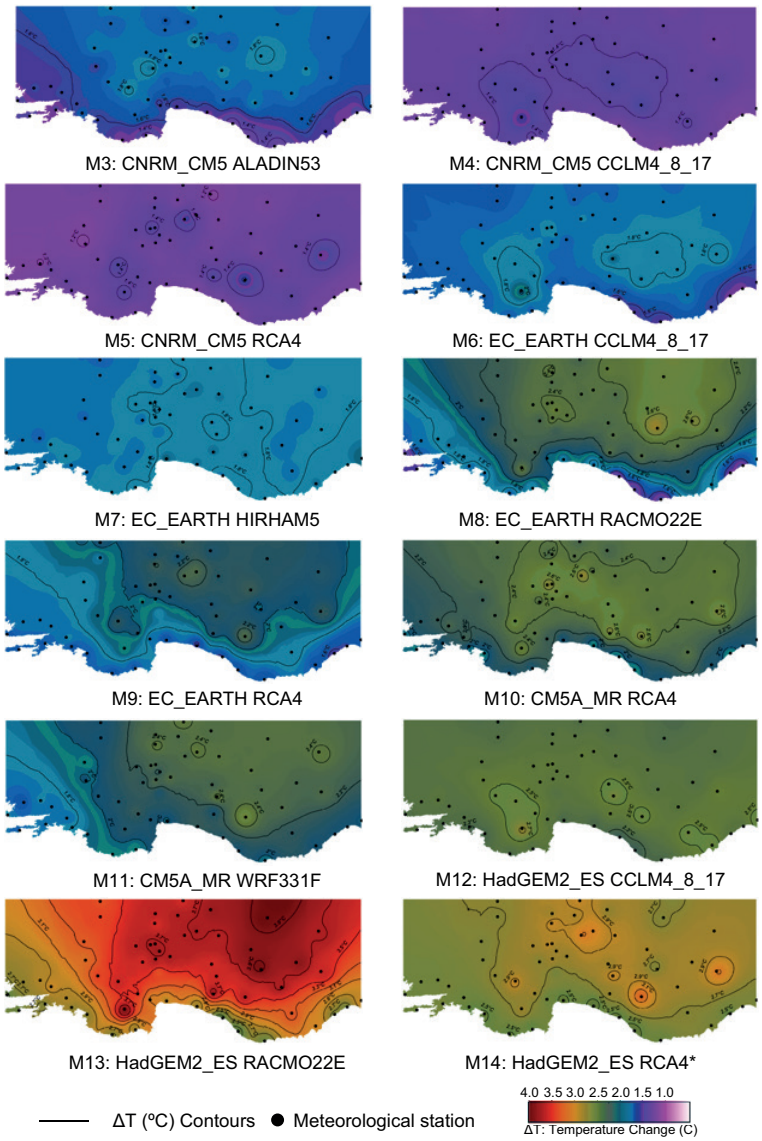

Fig. S10. Medium-term temperature change projections (RCP8.5) (ΔT_{annual} [ºC]) for models M3 through M14. All changes are verified to be statistically significant at the 95% confidence level. (*Best performing CORDEX model for the study area).

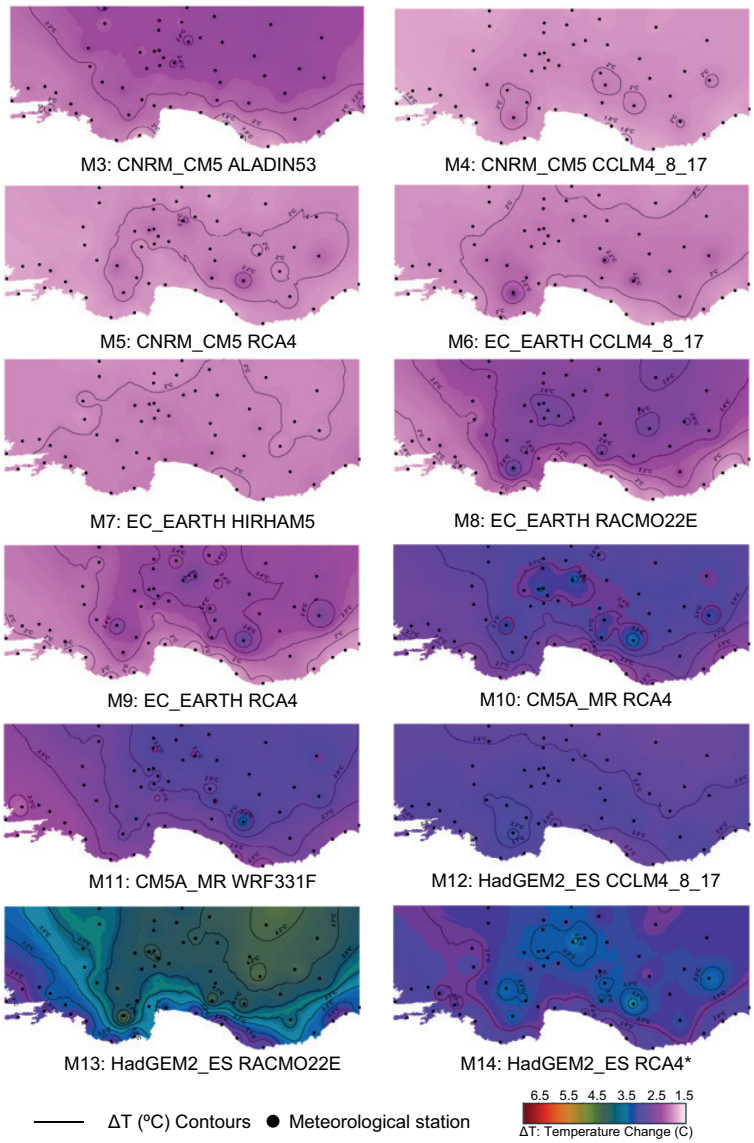

Fig. S11. Long-term temperature change projections (RCP4.5) (ΔT_{annual} [ºC]) for models M3 through M14. All changes are verified to be statistically significant at the 95% confidence level. (*Best performing CORDEX model for the study area).

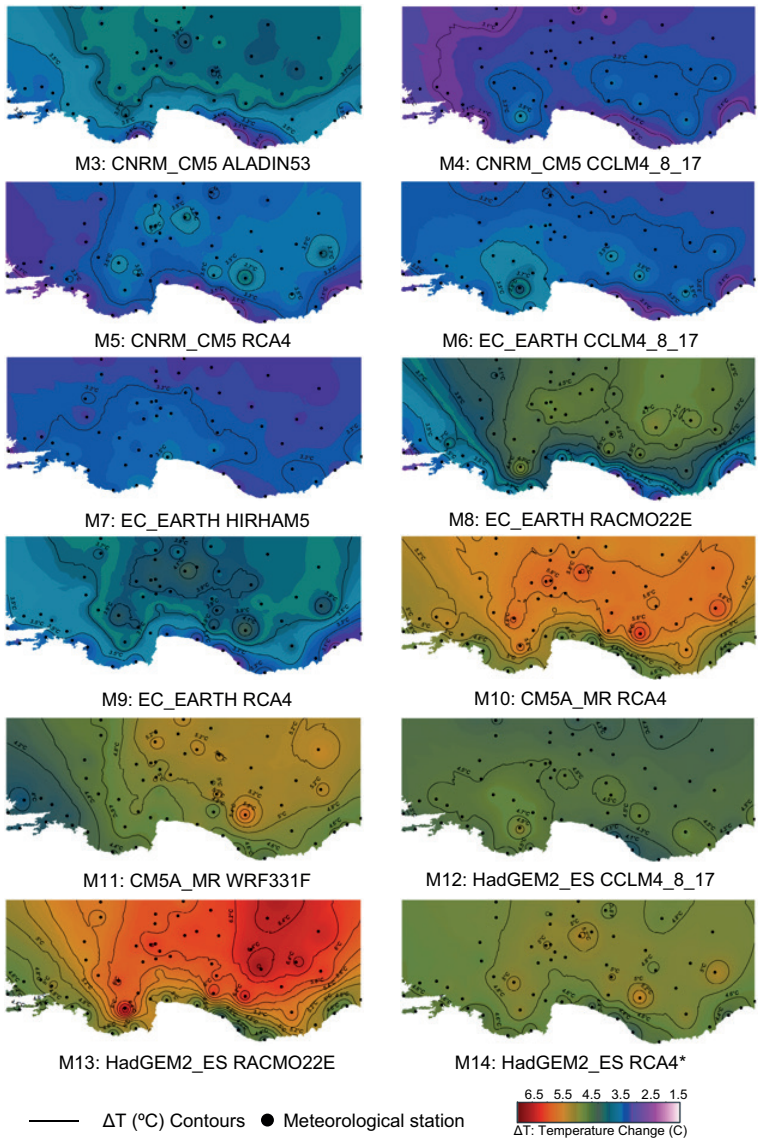

Fig. S12. Long-term temperature change projections (RCP8.5) (ΔT_{annual} [ºC]) for models M3 through M14. All changes are verified to be statistically significant at the 95% confidence level. (*Best performing CORDEX model for the study area).

S.4 Projections on seasonal temperature climatology

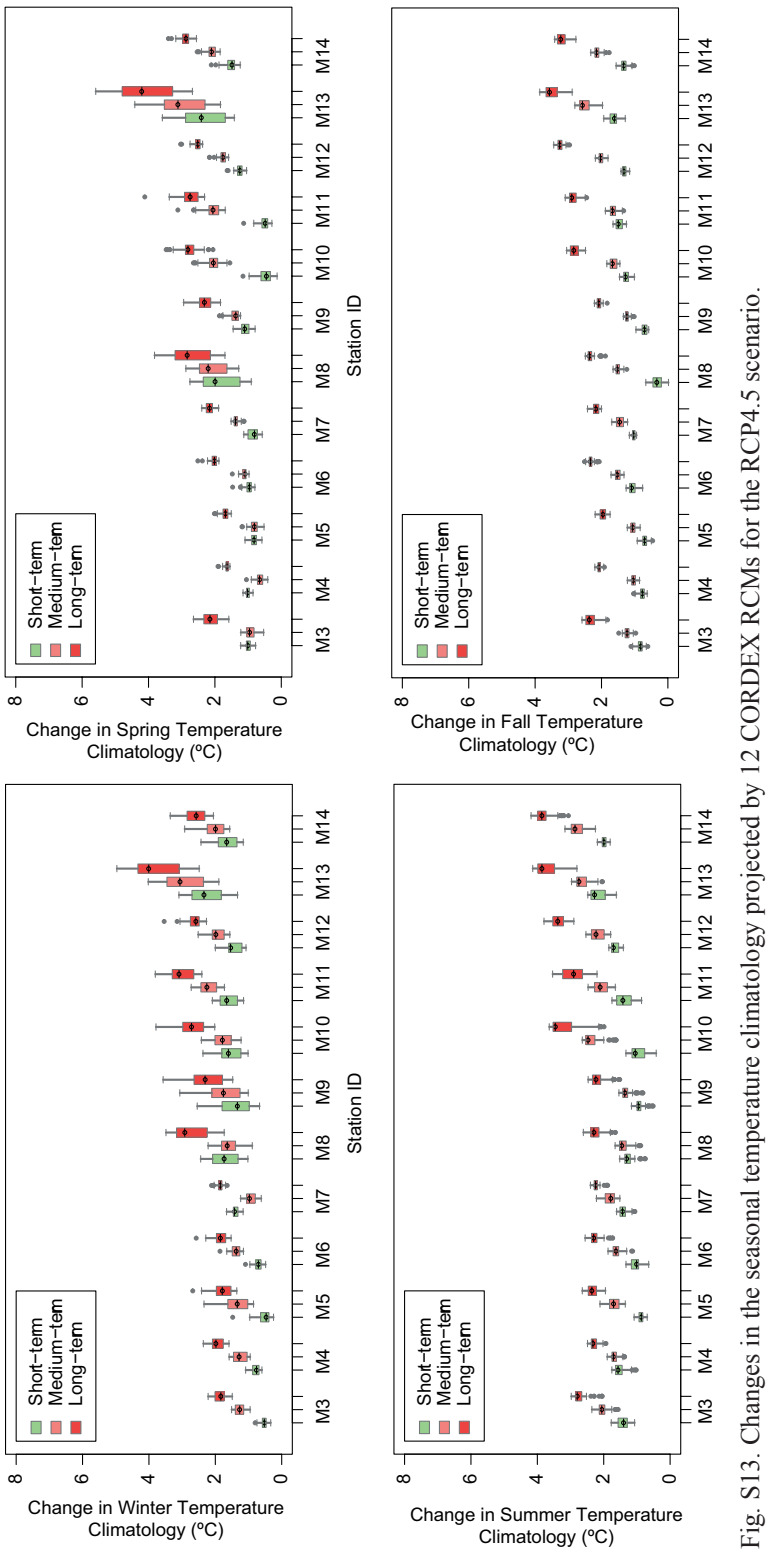

Fig. S13. Changes in the seasonal temperature climatology projected by 12 CORDEX RCMs for the RCP4.5 scenario.

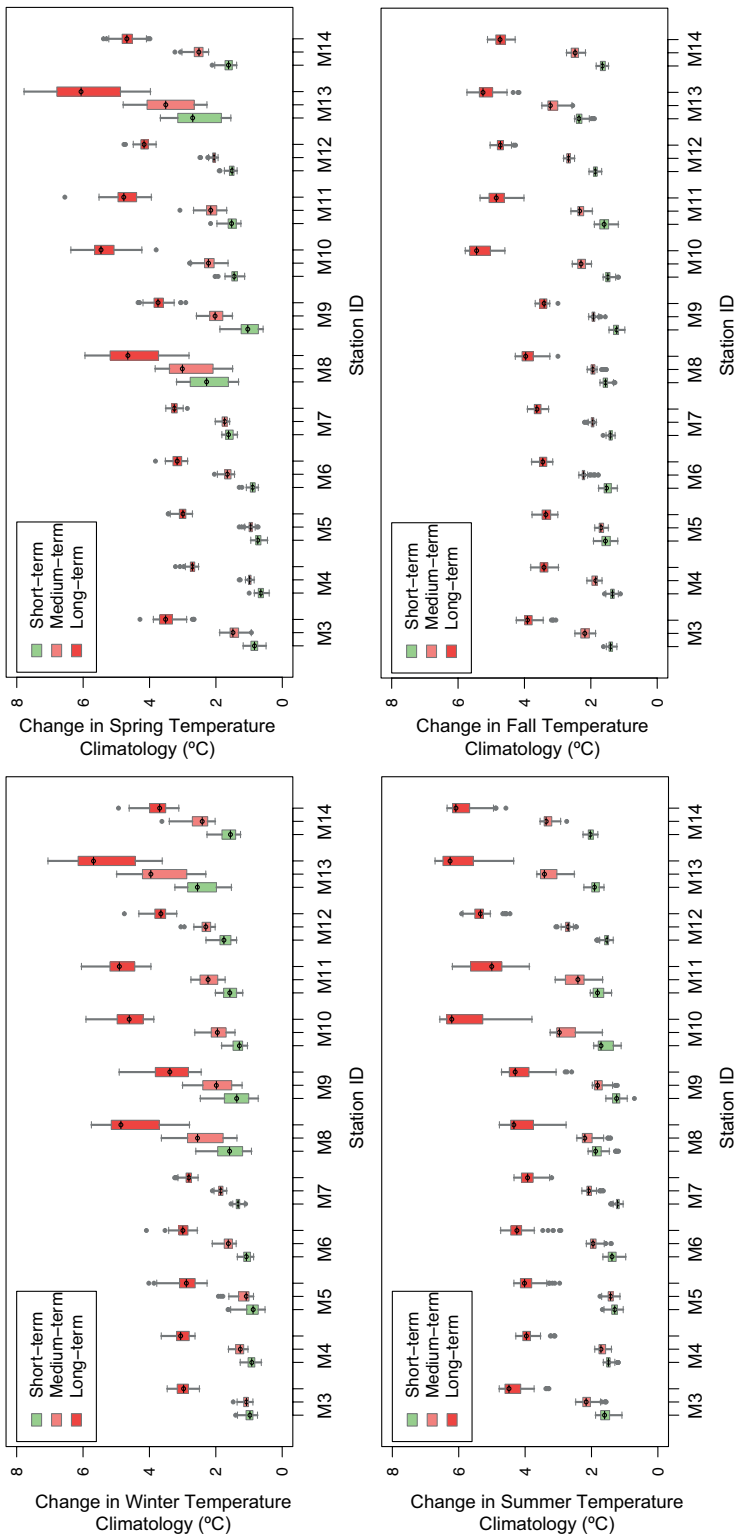

Fig. S14. Changes in the seasonal temperature climatology projected by 12 CORDEX RCMs for the RCP8.5 scenario.

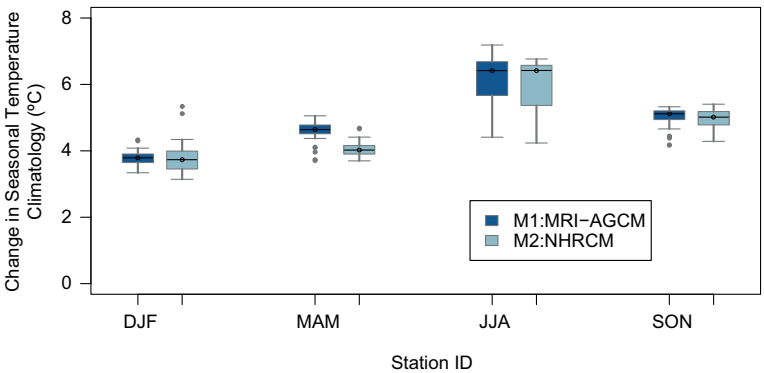

Fig. S15. Change in the seasonal temperature climatology (2080-2099) projected by MRI climate models for the RCP8.5 scenario.